

Mosquito vector competence for dengue is modulated by insect-specific viruses

Nature Microbiology

Olmo, Roenick P.; Tadjro, Yaovi M.H.; Aguiar, Eric R.G.R.; de Almeida, João Paulo P.; Ferreira, Flávia V. et al

<https://doi.org/10.1038/s41564-022-01289-4>

This publication is made publicly available in the institutional repository of Wageningen University and Research, under the terms of article 25fa of the Dutch Copyright Act, also known as the Amendment Taverne.

Article 25fa states that the author of a short scientific work funded either wholly or partially by Dutch public funds is entitled to make that work publicly available for no consideration following a reasonable period of time after the work was first published, provided that clear reference is made to the source of the first publication of the work.

This publication is distributed using the principles as determined in the Association of Universities in the Netherlands (VSNU) 'Article 25fa implementation' project. According to these principles research outputs of researchers employed by Dutch Universities that comply with the legal requirements of Article 25fa of the Dutch Copyright Act are distributed online and free of cost or other barriers in institutional repositories. Research outputs are distributed six months after their first online publication in the original published version and with proper attribution to the source of the original publication.

You are permitted to download and use the publication for personal purposes. All rights remain with the author(s) and / or copyright owner(s) of this work. Any use of the publication or parts of it other than authorised under article 25fa of the Dutch Copyright act is prohibited. Wageningen University & Research and the author(s) of this publication shall not be held responsible or liable for any damages resulting from your (re)use of this publication.

For questions regarding the public availability of this publication please contact openaccess.library@wur.nl



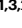



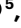


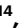
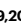




Mosquito vector competence for dengue is modulated by insect-specific viruses

Received: 10 August 2022

Accepted: 16 November 2022

Published online: 5 January 2023

 Check for updates

Roenick P. Olmo ^{1,2,22}, Yaovi M. H. Todjro ^{1,22}, Eric R. G. R. Aguiar ^{1,3,22}, João Paulo P. de Almeida ¹, Flávia V. Ferreira¹, Juliana N. Armache¹, Isaque J. S. de Faria ¹, Alvaro G. A. Ferreira⁴, Siad C. G. Amadou ¹, Ana Teresa S. Silva¹, Kátia P. R. de Souza¹, Ana Paula P. Vilela¹, Antinea Babarit², Cheong H. Tan ⁵, Mawlouth Diallo⁶, Alioune Gaye⁶, Christophe Paupy ⁷, Judicaël Obame-Nkoghe^{8,9}, Tessa M. Visser ¹⁰, Constantianus J. M. Koenraadt¹⁰, Merril A. Wongsokarijo¹¹, Ana Luiza C. Cruz¹², Mariliza T. Prieto¹³, Maisa C. P. Parra¹⁴, Maurício L. Nogueira ^{14,15}, Vivian Avelino-Silva¹⁶, Renato N. Mota¹⁷, Magno A. Z. Borges¹⁸, Betânia P. Drumond¹², Erna G. Kroon¹², Mario Recker ^{19,20}, Luigi Sedda ²¹, Eric Marois ², Jean-Luc Imler ² & João T. Marques ^{1,2} ✉

Aedes aegypti and *A. albopictus* mosquitoes are the main vectors for dengue virus (DENV) and other arboviruses, including Zika virus (ZIKV). Understanding the factors that affect transmission of arboviruses from mosquitoes to humans is a priority because it could inform public health and targeted interventions. Reasoning that interactions among viruses in the vector insect might affect transmission, we analysed the viromes of 815 urban *Aedes* mosquitoes collected from 12 countries worldwide. Two mosquito-specific viruses, Phasi Charoen-like virus (PCLV) and Humaita Tubiacanga virus (HTV), were the most abundant in *A. aegypti* worldwide. Spatiotemporal analyses of virus circulation in an endemic urban area revealed a 200% increase in chances of having DENV in wild *A. aegypti* mosquitoes when both HTV and PCLV were present. Using a mouse model in the laboratory, we showed that the presence of HTV and PCLV increased the ability of mosquitoes to transmit DENV and ZIKV to a vertebrate host. By transcriptomic analysis, we found that in DENV-infected mosquitoes, HTV and PCLV block the downregulation of histone H4, which we identify as an important proviral host factor in vivo.

Dengue fever is the fastest-growing vector-borne disease worldwide and causes an estimated 400 million new infections every year^{1–4}. In addition, over the past decades, several other arboviruses, including ZIKV and chikungunya (CHKV), have emerged and caused a substantial burden of disease. Increased transmission of arboviruses has been underpinned by increased geographic reach of the main vector mosquitoes, *Aedes aegypti* and *A. albopictus*^{4,5}, mainly due to climate change as warming produces ideal conditions for mosquitoes. Vector

abundance, assessed using cross-sectional surveys, has long been used as a proxy for infection risk, but the incidence of arbovirus infection does not directly correlate with mosquito abundance⁶. We still lack a complete understanding of the factors that affect rates of transmission to humans.

Virologic surveillance of adult *Aedes* mosquitoes by metagenomic analysis can lead to early identification of circulating arboviruses and help raise preparedness to inform public health measures that can

curtail or even prevent outbreaks⁷. In addition to arboviruses, these surveillance efforts have also identified an enormously diverse set of insect-specific viruses (ISVs) in *Aedes* mosquitoes^{8–12}. Although ISVs do not infect vertebrates, they have been shown to affect the capacity of the mosquito to be infected, maintain and transmit arboviruses, which together comprise vector competence and will therefore affect the incidence of infection in humans^{7,13,14}.

To carry out a comprehensive characterization of the viromes of mosquitoes that can harbour arboviruses, and inform risk assessment and public health strategies to mitigate arbovirus disease, we collected over 800 adult *Aedes* mosquitoes in the wild, performed metagenomic analysis and report our findings here.

Results

Virome analysis of *Aedes* mosquitoes

Adult *A. aegypti* and *A. albopictus* mosquitoes were collected from the field in 12 different sites from six countries on four continents (Fig. 1a). In total, 815 adult mosquitoes were pooled according to species, location and date of collection, resulting in 91 samples derived from 69 *A. aegypti* and 22 *A. albopictus*. Details of the pools are described in Supplementary Table 1. Whole mosquito samples were used to extract RNA and construct small RNA libraries that were sequenced and analysed using a shotgun metagenomic strategy previously optimized to detect viruses⁸. Briefly, this strategy is based on the detection of virus-derived small RNAs that are used to assemble longer contiguous sequences for further characterization. In total, we identified 1,448 putative viral contigs present in our mosquito samples (Fig. 1b,c). Data curation (described in Fig. 2a and in Methods) based on the phylogeny of polymerase genes (Fig. 2b) suggested that these contigs represent at least 12 different viruses, including 7 known viruses previously identified as ISVs. Out of these, 3 remain unclassified while the other 4 belong to the *Phenuiviridae*, *Xinmoviridae*, *Bunyaviridae* and *Flaviviridae* families (Fig. 2b). No known arboviruses were detected in our metagenomic analysis. The five remaining viral polymerase sequences showed low similarity to the closest known reference in Genbank. Phylogenetic analyses confirmed that they are probably new viral species (Extended Data Fig. 2) belonging to the *Partitiviridae*, *Totiviridae*, *Rhabdoviridae*, *Narnaviridae* and *Virgariidae* families (Fig. 2b). These viruses were named according to their classification (Fig. 2b). All new viruses were most closely related to known ISVs (Extended Data Fig. 2), but their final classification requires biological characterization.

All 12 identified viruses, 7 known and 5 new, had RNA genomes, either single-stranded (of positive and negative polarity) or double-stranded (Fig. 2b). The small RNA profile observed for these viruses shows clear production of small interfering RNAs (siRNAs) (Extended Data Fig. 3), which results from the activity of the RNAi pathway during active viral replication in the mosquito host^{8,15–19}. Viruses detected in *Aedes* mosquitoes were strictly species-specific and often associated with specific locations (Fig. 2c). Out of the 12 identified viruses, 10 were found in *A. aegypti* and 2 in *A. albopictus*, suggesting a less diverse virome in the latter even when accounting for a lower number of samples. Indeed, looking at the diversity of the mosquito virome per country, a single virus species was detected in each *A. albopictus* population, while 4–6 different viruses were present in *A. aegypti* (Fig. 2d). In addition, comparing different mosquito species that were collected from the same sites in Caratinga, Montes Claros, Lope, Franceville and Singapore, we observed that *A. aegypti* had higher virome diversity than *A. albopictus* in 4 out of 5 cases (Fig. 2c).

Using the small RNAs mapping to each virus contig as a proxy for abundance, we found that viral loads varied for the same virus in different locations and also between different viruses (Extended Data Fig. 4a). Detection of these new viruses in the original RNA samples from wild mosquitoes used for the metagenomic analysis was confirmed by reverse transcription quantitative PCR (RT-qPCR) and conventional PCR (Extended Data Fig. 4b,c). These results validated our small RNA

sequencing strategy. Detection of Orbis virgavirus (OVV) by RT-qPCR failed in samples from Suriname, but this was attributed to polymorphisms in the primer annealing region (Extended Data Fig. 4d). For each virus, the viral load determined by small RNA abundance corresponded with qRT-PCR detection. However, the relative quantification of viruses by qRT-PCR and small RNA abundance was unique for each virus, with some being underestimated (PCLV) or overestimated (Aslam narnavirus) (Extended Data Fig. 4e).

Biogeography of mosquito viruses

Three of 12 locations had 5 or more viruses circulating in the local *A. aegypti* population: Santos, Paramaribo and Singapore (Fig. 2c). Notably, these are all port cities, which are likely to have a continuous influx of mosquitoes. Three different lines of laboratory *A. aegypti* mosquitoes lacked any viruses according to our analysis (Fig. 2c). Most of the viruses we detected were present in mosquitoes at single sites but 5 were present on at least two continents (Fig. 2d). In *A. aegypti*, two known ISVs, PCLV and HTV, were present in more than half of the samples (Fig. 2c), with the remaining 8 viruses found in less than 20% of the samples. No viruses were found with a prevalence higher than 20% in *A. albopictus* and only one was present in multiple sites (Fig. 2c,d). HTV and PCLV in *A. aegypti* had the highest viral loads of all viruses in both mosquito species (Extended Data Fig. 4) but were not present in any samples of *A. albopictus*. Notably, HTV and PCLV were either absent, or were present at very low viral loads in *A. aegypti* mosquitoes collected in Africa (Fig. 2c), where transmission of arboviruses such as DENV and ZIKV is low (Extended Data Fig. 4f)^{1,2}. High loads of HTV and PCLV were observed in mosquitoes sampled in areas with high DENV/ZIKV incidence, namely Asia and South America (Extended Data Fig. 4f)^{1,2}. We hypothesized that there was a positive association between ISVs and arboviruses, which was unexpected since competition between RNA viruses in the same host would be more likely.

Circulation of ISVs and arboviruses in the wild

To examine the spatiotemporal dynamics of the two major resident viruses in wild mosquitoes, HTV and PCLV, we chose to focus on one of the 12 sites used for the metagenomic analysis, using a collection of archived mosquito RNA samples: 515 *A. aegypti* and 24 *A. albopictus*, previously collected over a period of 1 yr (August 2010 to July 2011) in Caratinga City, southeast Brazil (Fig. 3a). This dataset was previously used to assess DENV circulation in an endemic urban area²⁰. On the basis of our metagenomics approach, we detected 3 viruses in Caratinga mosquitoes: OVV, HTV and PCLV (Fig. 2c), which we confirmed using RT-qPCR. OVV, HTV and PCLV were detected in wild *A. aegypti* but were absent from *A. albopictus*, even though both species were often captured in the same traps (Fig. 3b). OVV was only detected in 3 individual mosquitoes, and we focused our analyses on HTV and PCLV, which were present at a prevalence of 61% and 85%, respectively (Fig. 3b,c). On the basis of this survey of individual mosquitoes by RT-qPCR, we confirmed that HTV and PCLV were highly prevalent in natural mosquito populations during the whole period of collection and independent of the location within the city (Fig. 3d and Extended Data Fig. 5a). Moreover, we observed a strong positive association between the presence of HTV and that of PCLV in mosquitoes ($P < 1 \times 10^{-10}$, chi-squared test), suggesting that co-infection might be advantageous for these viruses.

HTV and PCLV are presumed to be ISVs although they are poorly characterized so far^{8,21,22}. We detected HTV and PCLV in different tissues, including the salivary glands, which suggests that they could be transmitted by a mosquito bite (Extended Data Fig. 5b,c). To assess the possibility that HTV and PCLV could be transmitted to humans, we analysed human blood samples collected concomitantly with mosquitoes in Caratinga city, southeast Brazil from February to July 2011. Human blood samples and mosquitoes from Caratinga were previously analysed by RT-qPCR for the presence of DENV²⁰ and these data were used for comparison. Plotting the numbers of this previous analysis,

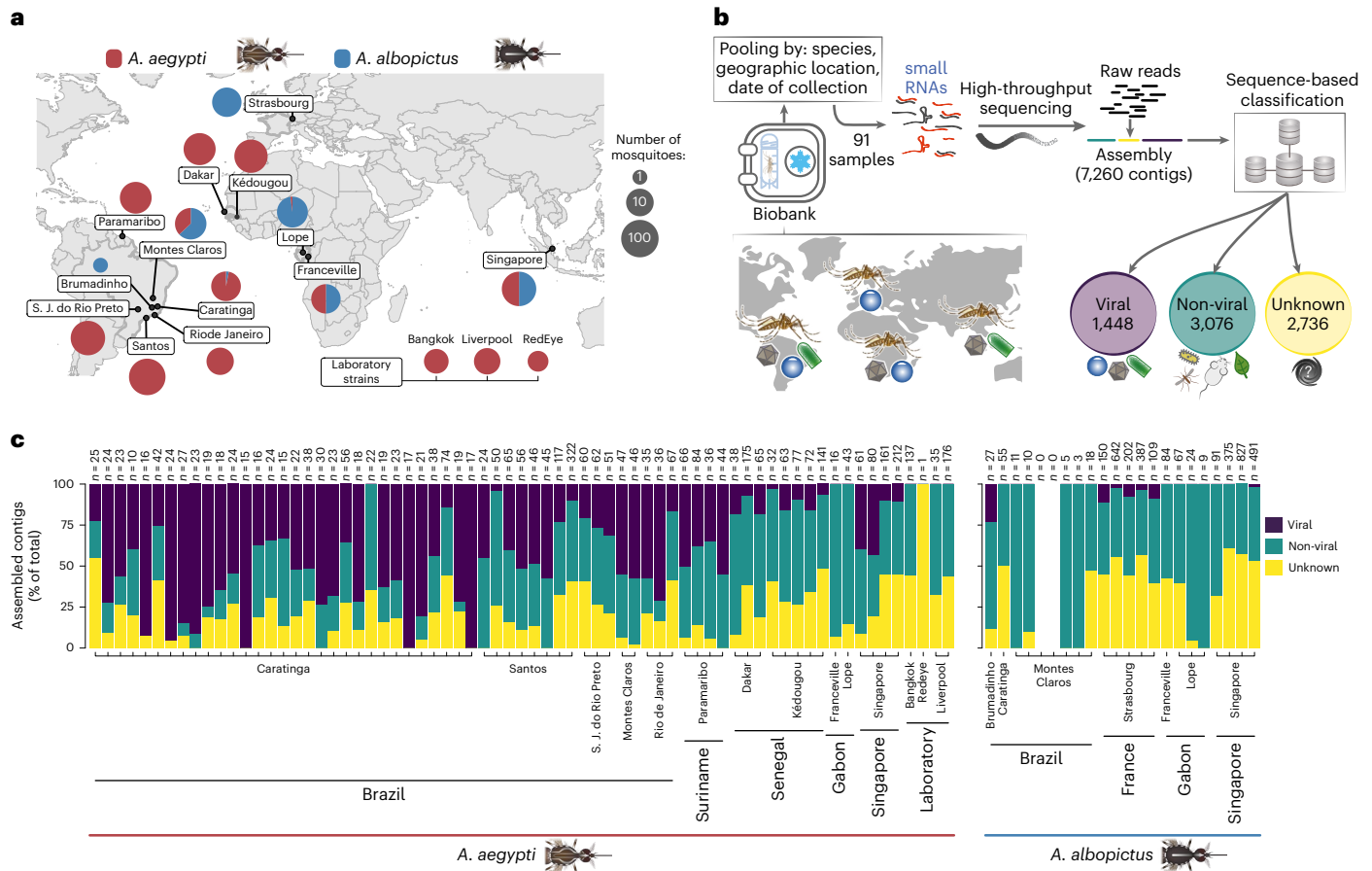


Fig. 1 | The virome of *A. aegypti* and *A. albopictus* mosquitoes. **a**, World map indicating sites of mosquito collection. Pie charts show the proportion of *A. aegypti* (red) and *A. albopictus* (blue) at each collection site. Adult mosquitoes were captured using either traps or human baits. Laboratory strains of mosquitoes analysed in this work are indicated at the bottom. **b**, Overview of our analysis pipeline. Captured mosquitoes were morphologically identified by species and stored in a biobank of RNA samples that were pooled to prepare small

RNA libraries for high-throughput sequencing. Using our metagenomic pipeline, assembled contigs were classified into viral and non-viral sequences on the basis of similarity against reference databases. Sequences that lack any similarity to known references are indicated as unknown. **c**, Individual results from our metagenomic analysis for each of the 91 small RNA libraries in this study. Bars indicate the total number of contigs and the proportion of viral, non-viral and unknown contigs per library.

we observe that DENV was detected in less than 5% of mosquitoes but was found in more than 30% of human blood samples (Fig. 3c). We did not detect HTV or PCLV in RNA extracted from human blood samples from Caratinga despite their high prevalence in mosquitoes, suggesting that these viruses are unable to productively infect humans (Fig. 3c). Furthermore, HTV and PCLV do not grow in mammalian cell lines, such as Vero cells, reinforcing the idea that they are ISVs (Extended Data Fig. 5d,e). HTV and PCLV were detected in mosquito eggs, which suggests that these viruses are maintained in mosquitoes by vertical transmission (Extended Data Fig. 5c).

Our data indicate that HTV and PCLV are not infectious to humans, but we wanted to understand whether they might affect how arboviruses are transmitted. In the dataset of mosquitoes from Caratinga City analysed here, we observed a statistically significant enrichment of HTV and PCLV in individuals that also harboured DENV (Fig. 3e). Statistical analyses revealed that both HTV alone (Odds ratio (OR) 2.59; 95% Confidence interval (CI): 1.09, 716) and HTV/PCLV co-infections (OR 3.06; 95% CI 1.29, 8.46) are both associated with the presence of DENV in mosquitoes, whereas PCLV alone had no statistically significant association with DENV. However, due to the positive association between HTV and PCLV that we identified in mosquitoes from Caratinga ($P < 1 \times 10^{-10}$, chi-squared test, described above), it is hard to dissect the contribution of each virus. We note that our analysis is based on a small sample of mosquitoes, which could be affected by physical, ecological

or environmental factors. However, in Caratinga, a town that is only 3 km wide and 3 km long, ecological conditions are probably homogeneous on the same collection date. Mosquito population density was not found to be important for DENV transmission in a previous study from our group²³. In addition, our analyses found neither geographic nor temporal patterns of virus distribution in Caratinga (Fig. 3d and Extended Data Fig. 5a). Thus, our observations using field samples strongly indicate a positive interaction between the two ISVs (HTV and PCLV) and the arbovirus DENV in mosquitoes.

HTV and PCLV increase arbovirus replication in mosquitoes

Since we had access to ovitraps from Rio de Janeiro where HTV and PCLV were also found at high prevalence, we obtained a few hundred eggs from wild *A. aegypti* mosquitoes and reared them in the laboratory for 2 generations. From the F₂ of the lab-reared population, we pooled eggs from 5 individual females that were either free of any virus or carried both HTV and PCLV to produce two separate mosquito lines (see Methods for details). We were unable to isolate lines carrying only HTV or PCLV, reinforcing the strong association observed in our wild sample cohort.

We exposed the two separate mosquito lines that were ISV-free or co-infected with HTV/PCLV to blood feeding on mice previously infected with DENV or ZIKV using an infectious blood meal. We found that mosquitoes carrying HTV and PCLV had similar prevalence and viral loads of DENV in the midgut at 4, 8 and 14 d.p.f. (days post feeding)

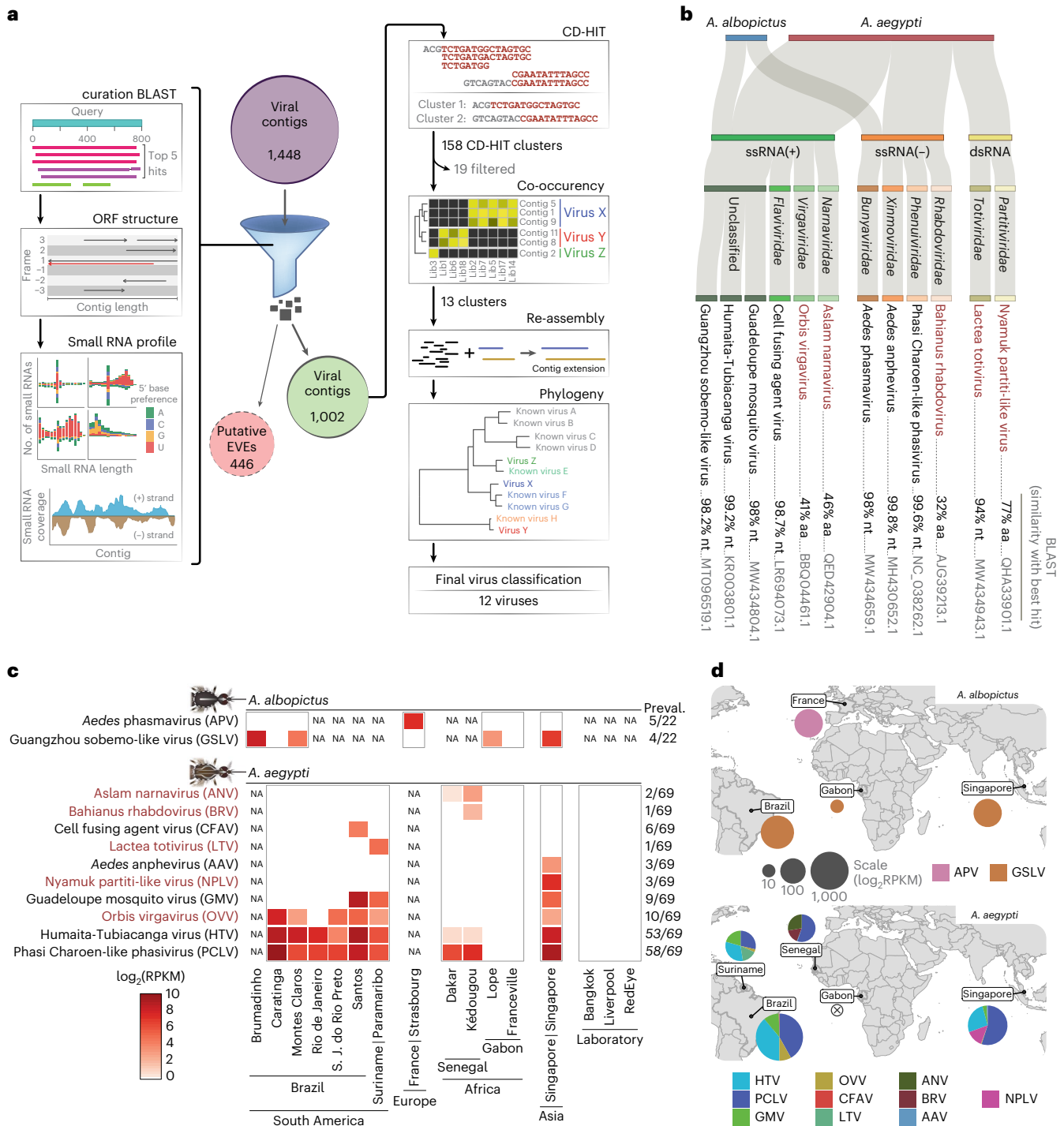


Fig. 2 | A highly diverse and distinct collection of viruses in *A. aegypti* and *A. albopictus*. **a**, Overview of the strategy for manual curation of viral contigs to confirm the origin and remove sequences potentially derived from EVEs. Curation consisted of BLAST search for similar viral sequences, inspection of predicted ORF structure including continuity and extension throughout each contig, and evaluation of the small RNA profile for the identification of signatures of siRNA production (symmetrical accumulation of RNAs with 20–23 nt length that mapped to each strand with no 5' base preference) or piwi interacting RNA (piRNA) production (accumulation of 24–29 nt length RNAs with 5' U preference); and overall contig coverage by small RNAs. Remaining viral contigs were clustered by sequence similarity and co-occurrence to identify groups of contigs that belong to the same viruses. Re-assembly was performed within these groups and resulting contigs were analysed for the presence of domains. Potential polymerases identified were used to classify viruses on the basis of sequence similarity and phylogeny. **b**, Host, virus genomic organization,

family and closest reference on GenBank identified by BLAST similarity searches for each of the 12 viruses identified in our datasets. New viral species are indicated in red, while previously known viruses are in black. Sequence similarity and accession number according to the closest viral sequence at the nucleotide (nt) or protein (aa) level are indicated. **c**, Viral load shown as a heat map for each of the 12 viruses in mosquito populations from each collection site or laboratory strain. In the heat map, white indicates absence of a virus and NA indicates absence of samples from a given location. Prevalence of each virus is shown on the right as number of samples with detectable virus over the total. Number of individuals per pool and number of species per collection site are described in Supplementary Table 1. RPKM, reads per kilobase of transcript per million reads mapped. **d**, Pie charts of the overall burden of virus and viral diversity for *A. aegypti* and *A. albopictus* populations in each collection site across the world. ⊗ indicates no viral contigs identified.

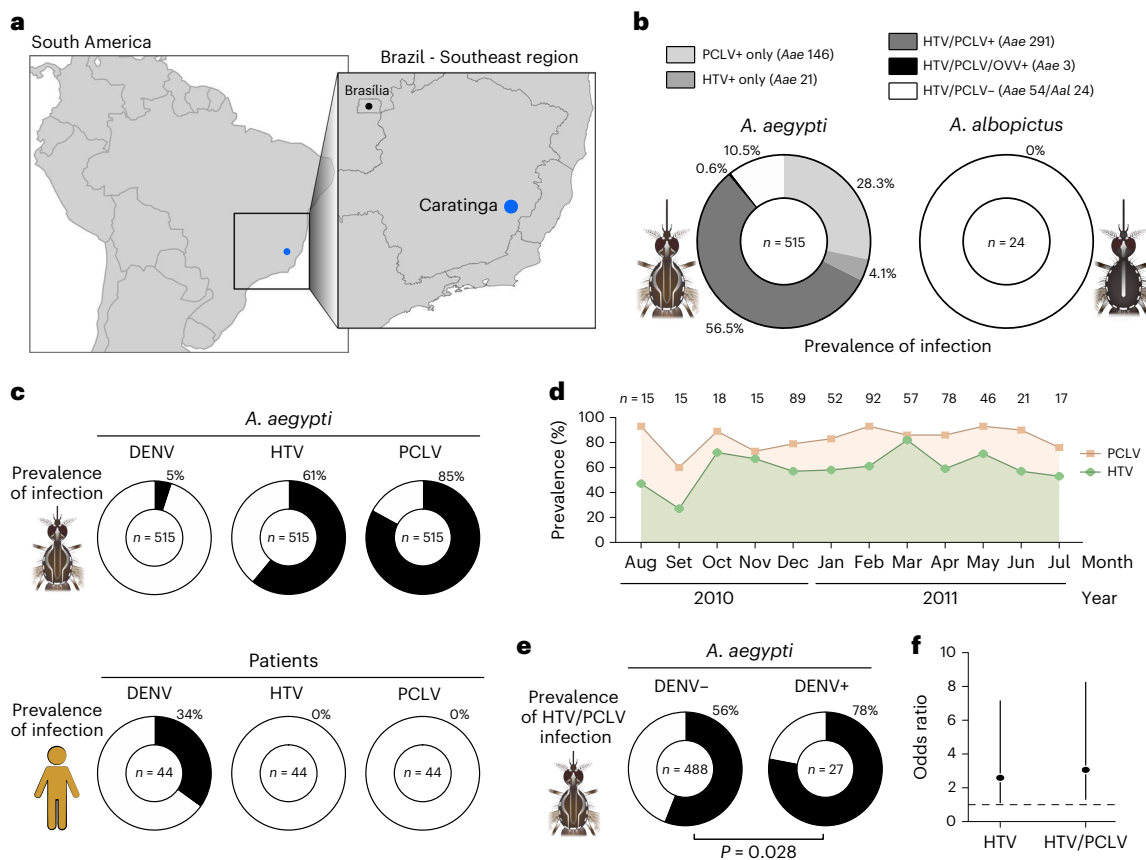


Fig. 3 | Concurrent detection of HTV, PCLV and DENV. **a**, Location of the study site, the city of Caratinga in the Southeast of Brazil. **b**, Prevalence of individual and co-infections by OVV, HTV and PCLV tested by RT-qPCR. **c**, Prevalence of DENV, HTV and PCLV separately in individual *A. aegypti* mosquitoes and human blood samples assessed by RT-qPCR. **d**, Monthly prevalence of HTV and

PCLV separately in individual *A. aegypti* mosquitoes. **e**, Prevalence of HTV and PCLV co-infection in DENV-infected (DENV+) and DENV non-infected (DENV-) mosquitoes. Statistical significance was determined by two-tailed Fisher's exact test. **f**, Likelihood of DENV infection in mosquitoes carrying HTV or PCLV and HTV shown by odds ratio. The dashed line shows odds ratio of 1.

as ISV-free mosquitoes (Fig. 4a,b). At 14 d.p.f., we observed a trend towards higher viral load of DENV in the midgut of mosquitoes carrying HTV/PCLV, but this trend was not statistically significant (Fig. 4b). In the carcass of mosquitoes, we observed a 5-fold significant increase in DENV levels at 8 and 14 d.p.f. in individuals carrying HTV/PCLV compared with ISV-free controls (Fig. 4c). Mosquitoes with HTV/PCLV also displayed higher susceptibility to ZIKV than ISV-free mosquitoes (Fig. 4d-f). ZIKV RNA levels were significantly increased at 4, 8 and 14 d.p.f. in the midgut of mosquitoes carrying HTV and PCLV compared with ISV-free controls (Fig. 4e). In the carcass, we observed a 5-fold increase in dissemination at 4 d.p.f. and significantly 10-fold higher viral loads at 8 d.p.f. in the presence of HTV and PCLV. Overall, our results demonstrate increased systemic DENV and ZIKV infection in mosquitoes carrying HTV/PCLV compared with virus-free controls.

To further investigate the specific effect of HTV and PCLV during the systemic phase of infection, we directly injected ZIKV into the mosquito haemocoel, which bypasses the stage of midgut infection (Extended Data Fig. 6a). Here we also observed increased viral replication in the carcass of HTV/PCLV-carrying wild mosquitoes compared with ISV-free controls (Extended Data Fig. 6a-c).

Our mosquito colonies established from individuals with and without ISVs were derived from the same but highly heterogeneous wild population. It is therefore possible that our selection generated colonies composed of individuals that differed with regards to their genetic backgrounds in addition to the presence of ISVs. To rule out a role for the genetic background, we next performed experiments with laboratory mosquitoes that are genetically more homogeneous. Laboratory

mosquitoes were artificially infected with HTV and PCLV to test whether ISVs have a direct impact on susceptibility to arboviruses (Extended Data Fig. 6d). Notably, HTV and PCLV loads and tissue tropism during artificial injection were similar to those of naturally infected mosquitoes after 8 d.p.i. (days post injection) (Extended Data Fig. 5b). Artificially infected laboratory mosquitoes had increased systemic ZIKV RNA levels at 8 d.p.f. (Extended Data Fig. 6d-f) compared with controls, similar to what we observed for lines carrying HTV and PCLV derived from wild populations. Increased systemic viral replication was also observed when laboratory mosquitoes were artificially infected with HTV and PCLV before being injected with ZIKV (Extended Data Fig. 6g-i). Although artificially infected lab mosquitoes did not show increased ZIKV replication in the midgut, this can be explained by the fact that naturally infected mosquitoes have more marked effects due to the presence of HTV and PCLV throughout development (Extended Data Fig. 5b).

Notably, in wild mosquitoes, ZIKV infection had a positive impact on PCLV levels in the midgut of infected mosquitoes (Extended Data Fig. 6j,k), which suggests a mutual beneficial interaction between these viruses. As mentioned before, HTV was not detected in the midgut even in the presence of ZIKV (Extended Data Fig. 6l). Neither HTV nor PCLV was consistently affected by ZIKV infection in the carcass, although we observed an increase in PCLV levels and a reduction in HTV levels in single time points (Extended Data Fig. 6m,n).

Transmission of DENV and ZIKV is increased by ISVs

We tested whether increased ZIKV and DENV levels in mosquitoes carrying HTV and PCLV led to increased amounts of arboviruses in

mosquito salivary glands, and increased transmission to a vertebrate host. Wild HTV/PCLV-positive mosquitoes showed faster kinetics and higher prevalence of ZIKV infection in salivary glands compared with ISV-free controls (Fig. 4g and Extended Data Fig. 6o,p). We simulated vectorial transmission in a susceptible animal model using mice deficient in type I and type II interferon receptors^{24,25} (Fig. 4h). We opted to test ZIKV transmission because the mouse model for this virus is more robust than for DENV. Mice were incubated with ZIKV-infected mosquitoes at 6, 8 and 12 d.p.f. and viremia was analysed in these animals. No viremia was observed in mice bitten by mosquitoes at 6 d.p.f. (Fig. 4i). Mosquitoes were able to efficiently transmit ZIKV to 5 out of 5 mice at 8 d.p.f. but only in the presence of HTV and PCLV (Fig. 4i). At 12 d.p.f., mosquitoes with or without HTV/PCLV were able to equally transmit ZIKV to 3 out of 3 mice (Fig. 4i). Thus, the presence of ISVs is associated with shortening of the extrinsic incubation period (EIP) of ZIKV, which is the time required for infected mosquitoes to become infectious to a vertebrate host. While mosquitoes carrying HTV and PCLV were able to transmit ZIKV between 7 and 8 d, ISV-free individuals required between 9 and 12 d. Thus, the presence of ISVs in mosquitoes could lead to shortening of the EIP between 1 and 5 d, although our experiments did not allow us to pinpoint the exact difference. Furthermore, mosquitoes carrying HTV and PCLV and analysed at both 8 and 12 d.p.f. had significantly higher ZIKV levels compared with ISV-free controls (Fig. 4j).

To further elucidate the impact of HTV and PCLV infection on the EIP, we applied a previously developed mathematical model^{26,27}. Our modelling demonstrates that even small changes in EIP could have a large impact on the number of human infections (Fig. 4k). For example, shortening the EIP from 10 d to 8 d, within the range of the difference we observed between mosquitoes with and without ISVs in the laboratory, could lead to a 5-fold increase in the number of infections (Fig. 4k), which can be explained by the short average life expectancy of *Aedes* mosquitoes in the wild. Consequently, arboviral prevalence in mosquitoes is also increased due to both the increased availability of infected humans and faster viral kinetics inside mosquitoes (Fig. 4l), providing a link between our field observations and laboratory experiments. Although this model was parameterized for DENV transmission, the results should broadly hold for other arboviral diseases transmitted by the same mosquito vector, including ZIKV.

HTV and PCLV modulate histone H4 expression in mosquitoes

To probe the biological mechanisms by which ISVs affect systemic dissemination of arboviruses in *A. aegypti* mosquitoes, we analysed the transcriptome of RNA collected from entire mosquito carcasses at different times after DENV infection (4, 8 and 14 d.p.f.). Overall, we found that the presence of HTV and PCLV had little effect on the transcriptome of DENV-infected mosquitoes (Extended Data Fig. 7a). Only 100/10,000 genes analysed were significantly up- or downregulated and less than 10 were common between time points (Extended

Data Fig. 7b). Of interest, genes associated with known antiviral pathways, such as Toll, IMD, Jak-STAT, autophagy and RNA interference did not show any consistent differences in expression (Extended Data Fig. 7c). Next, we compared the transcriptome of DENV-infected and non-infected individuals from groups of mosquitoes carrying HTV and PCLV, or virus-free controls, using gene set enrichment analysis (GSEA)²⁸ (Fig. 5a). We focused our analysis on the carcass of mosquitoes infected by DENV at 8 and 14 d.p.f. where the presence of HTV and PCLV had the strongest effect (Fig. 5a). This analysis identified 7 biological pathways that were significantly affected both by the presence of HTV/PCLV and DENV infection in at least one time point (Fig. 5b). Notably, all pathways were downregulated during DENV infection and upregulated by the presence of HTV and PCLV, as indicated by the enrichment score (NES) (Fig. 5b). Out of these, four pathways were significantly affected in at least 6 out of 8 comparisons: *nucleosome*, *nucleosome assembly*, *DNA templated transcription initiation* and *protein heterodimerization activity* (Fig. 5b). Analysis of genes responsible for the significant enrichment showed that they were almost the same for these 4 biological pathways (Fig. 5c). Indeed, histones represented the majority of genes differentially regulated by DENV infection and the presence of HTV and PCLV, with histone H4 topping the list (Fig. 5c). Thus, we used RT-qPCR to analyse histone H4 expression and validate our observations in independent experiments using ZIKV. Histone H4 expression was significantly downregulated by ZIKV infection in the carcass of infected mosquitoes in a time-dependent manner (Fig. 5d,e), which was prevented by the presence of HTV and PCLV (Fig. 5e). Furthermore, levels of histone H4 were significantly higher in the presence of HTV and PCLV at every time point tested, compared with ISV-free controls (Fig. 5e). We also observed upregulation of histone H4 in the midgut, but only at 4 d.p.i. (Extended Data Fig. 7d,e). Importantly, differential expression of histone H4 between mosquitoes with or without HTV/PCLV was only observed in the presence of DENV and ZIKV infections (Fig. 5f,g). We also show that artificial infection of laboratory mosquitoes with HTV and PCLV alone did not significantly affect histone H4 expression (Extended Data Fig. 7f,g).

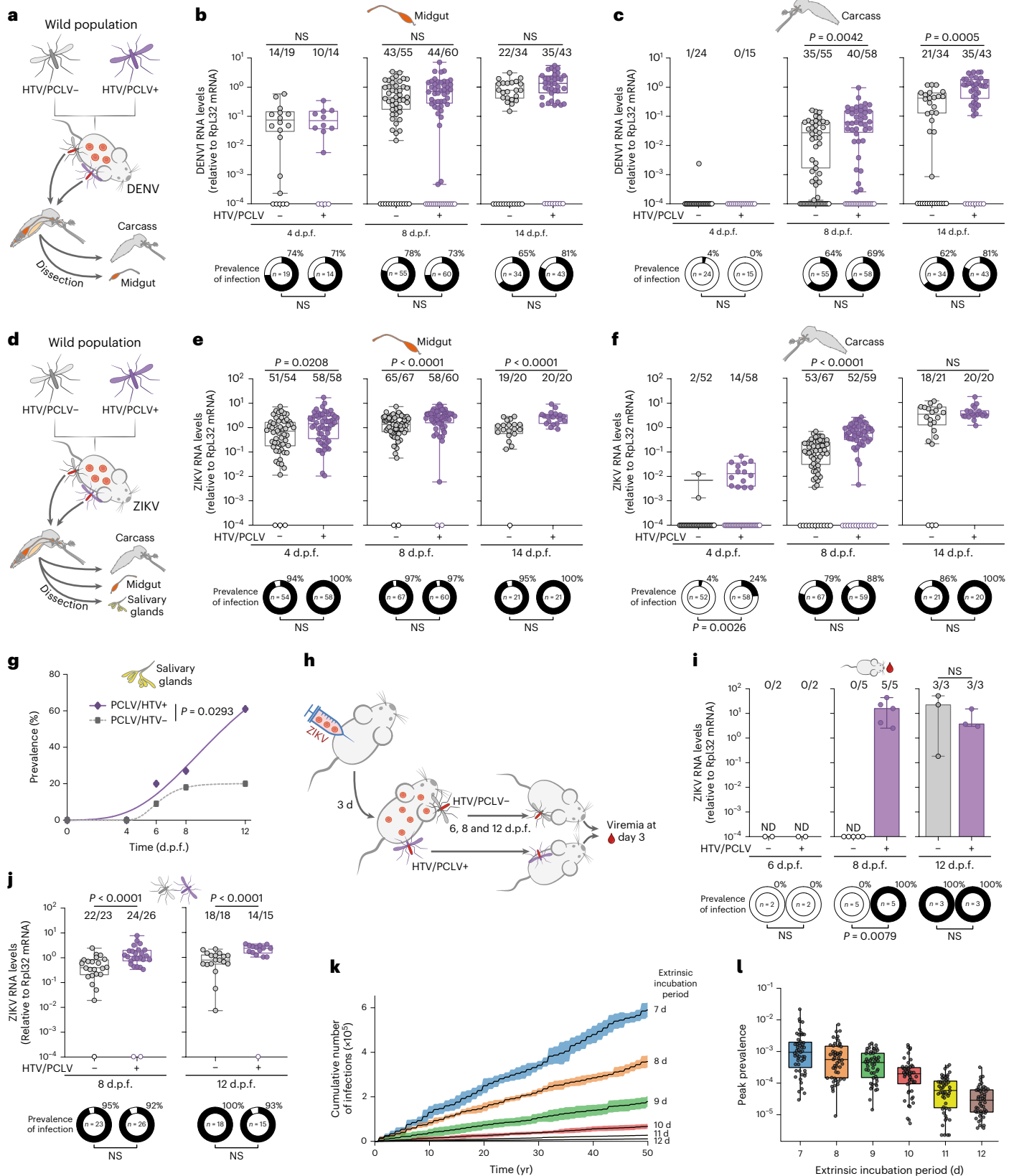
Histone genes are highly conserved and are often found in multiple copies that lack polyadenylation signals²⁹. Yet, there are non-canonical histone genes that possess polyadenylation signals. The genome of *A. aegypti* encodes at least 299 histone genes in the assembled chromosomes (chr.) and another 135 copies present in extra supercontigs (Extended Data Fig. 8a). In comparison, humans encode only about 80 histone genes in total²⁹ despite having a larger genome. Most histone genes of *A. aegypti* (267 out of 299) were found in a single cluster on chr. 3 (Extended Data Fig. 8a,b). With regards to histone H4, we identified 66 genes in total and 59 in the cluster on chr. 3 (Extended Data Fig. 8a). Histone H4 genes showed high similarity with almost 100% amino acid conservation, but also showed some sequence variation at the nucleotide level, especially in the copies outside of the chr. 3 cluster

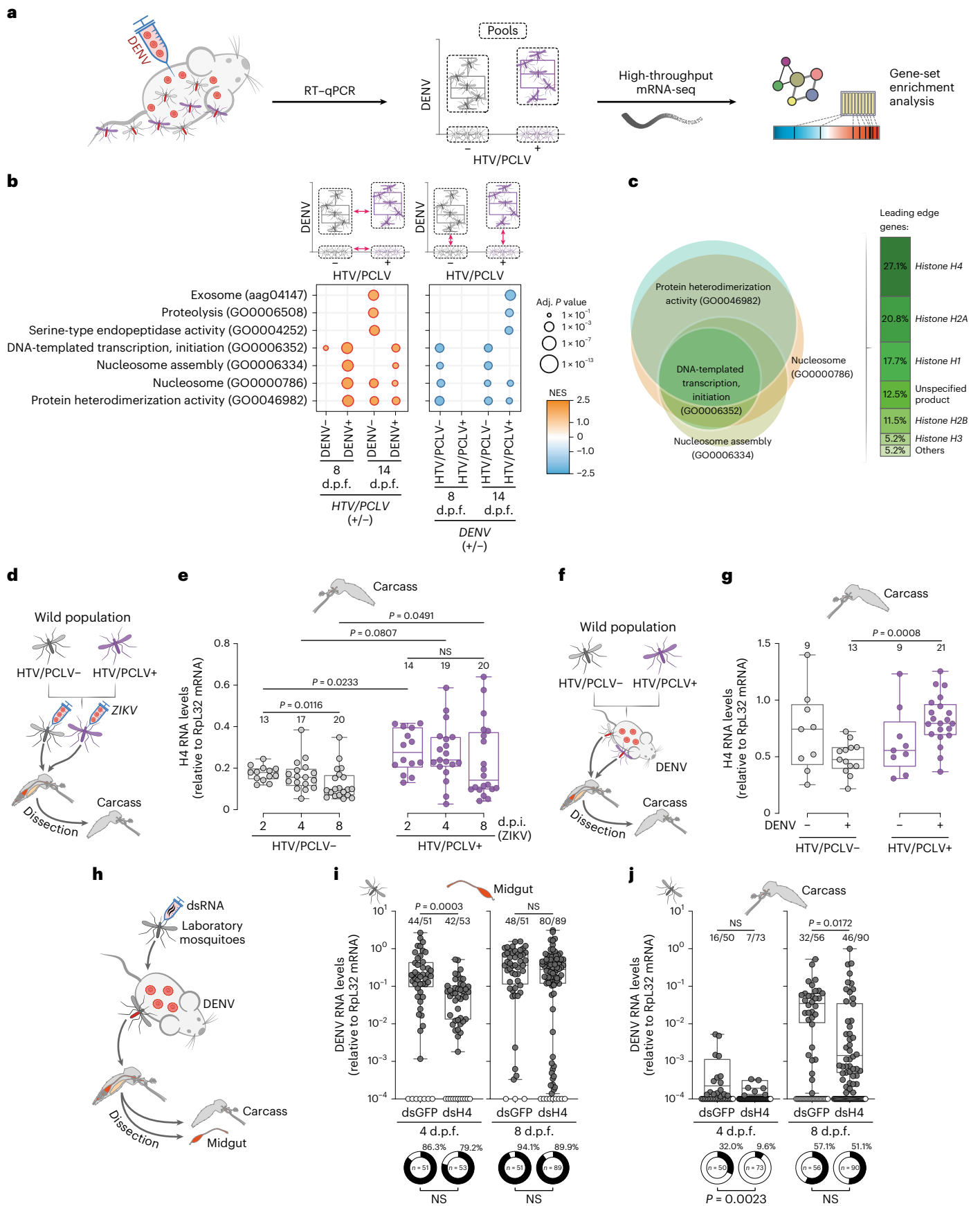
Fig. 4 | Effects of insect-specific viruses on DENV and ZIKV transmission. a–g, Strategy to evaluate the interference of HTV and PCLV on DENV (a–c) or ZIKV (d–g) infection in wild mosquito populations. HTV/PCLV-infected or virus-free mosquitoes were exposed to DENV (a) or ZIKV (d) on a blood meal. Viral loads and prevalence of infection were measured in the midgut (b,e), carcass (c,f) and salivary glands (g) of mosquitoes at the indicated d.p.f. Pie charts below each group indicate the prevalence of DENV or ZIKV infection at each time point. h, Strategy to compare the ability of mosquitoes with or without HTV and PCLV to transmit ZIKV to the susceptible AGL29 mouse model. i, Viremia in mice was determined 3 d after exposure to mosquito bites, comparing animals that were bitten by mosquitoes carrying or not carrying HTV and PCLV at 6, 8 and 12 d post oral infection. Bars represent the median and the error shows maximum and minimum values. ND, not detected. NS, non-significant. Pie charts below each group indicate the prevalence of infection. j, ZIKV RNA levels in mosquitoes used in the transmission experiment in i. k,l, Spatially explicit, individual-based

meta-population model showing the effect of EIP duration on the number of human infections (k) and virus prevalence in mosquitoes (l) taken as a proportion of infected individuals on a single day during the seasonal peak over a 50 yr period ($n = 50$). In boxplots of b, c, e, f, j and l, boxes show the second and third interquartile ranges divided by the median, while whiskers represent maximum and minimum values. Statistical significance was determined by two-tailed Mann–Whitney *U*-test. In k, lines represent the averaged cumulative incidence over five model runs for each value of the EIP, while shadows depict confidence intervals. Numbers of infected midguts (b,e), carcasses (c,f) or whole mosquitoes (j) over the total number tested are indicated above each column. Each dot represents an individual sample. Statistical significance of the prevalence of infection was determined in b, c, e, f, i and j using two-tailed Fisher's exact test or, in g, using a binomial generalized linear model followed by type II ANOVA testing with time points as factor.

(Extended Data Fig. 8c,d). Histone H4 genes that have clear polyadenylation signals were the most detected in our dataset and in the available transcriptome of mosquito tissues since they were all prepared using polyA selection (Extended Data Fig. 8d). Interestingly, the effect of HTV and PCLV on histone H4 RNA levels was not significant when we

analysed polyadenylated copies, which represented less than 10% of all histone H4 expression (Extended Data Fig. 8e). This suggests that HTV and PCLV may primarily affect non-polyadenylated histones that are coordinately synthesized with DNA replication during the S-phase of cell division and are stable after incorporation into chromatin³⁰.





Silencing of histone H4 and DENV replication in mosquitoes
 We applied double stranded RNA (dsRNA)-mediated gene silencing to knock down histone H4 expression in adult mosquitoes before infection

with DENV or ZIKV (Fig. 5h and Extended Data Fig. 8f,g). Mosquitoes silenced for histone H4 before infection had significantly reduced DENV levels in the midgut at 4 and 8 d.p.i., although the difference was

Fig. 5 | HTV and PCLV regulate the expression of proviral histone H4 during DENV infection. **a**, Overall strategy to identify biological pathways associated with HTV and PCLV interaction with DENV. HTV/PCLV-infected and virus-free wild mosquito populations were allowed to feed on DENV-infected mice. The transcriptome of DENV-infected and non-infected mosquitoes from HTV/PCLV and virus-free groups were analysed separately at 8 and 14 d.p.f. GSEA was performed for each comparison. **b**, Biological processes significantly enriched (adjusted $P < 0.01$) in the comparisons of DENV-infected versus non-infected mosquitoes and PCLV/HTV-infected versus virus-free controls are shown. **c**, Overlap of leading-edge genes belonging to the 4 biological processes enriched in at least 6 out of 8 comparisons. Size of each circle represents the number of leading-edge genes. Histogram shows that histone genes represent the majority in the leading edge of significantly enriched processes. **d, e**, Experimental design (**d**) and histone H4 levels in the carcass of wild mosquitoes carrying HTV/PCLV and infected with ZIKV vs virus-free controls

at 2, 4 and 8 d.p.i. (**e**). **f, g**, Experimental design (**f**) and differential expression of histone H4 levels in the carcass of mosquitoes in the presence of HTV and PCLV is only observed in DENV-infected individuals (**g**). **h–j**, Experimental design (**h**) and silencing of histone H4 mRNA in adult mosquitoes exposed to DENV. DENV infection was analysed at 4 and 8 d.p.f. in the midgut (**i**) and carcass (**j**) of silenced (dsH4) and control (dsGFP) mosquitoes. Pie charts below each group indicate the prevalence of DENV or ZIKV infection. In boxplots of **e, g, i** and **j**, boxes show the second and third interquartile ranges divided by the median while whiskers represent maximum and minimum values. Numbers of infected samples over the total number tested are indicated above each column. Statistical significance was determined by two-tailed one-way ANOVA with Tukey's correction for multiple comparisons (**e, g**) or by two-tailed Mann–Whitney U -test (**i, j**). Each dot represents an individual sample. Statistical significance of prevalence of infection was determined by two-tailed Fisher's exact test.

not significant at the later time point (Fig. 5i). As a result, we observed slower kinetics of infection in the carcass with lower prevalence at 4 d.p.i. and reduced viral loads at later time points (Fig. 5j). These results indicate that histone H4 is an important proviral host factor during DENV infection. As observed for the effect of HTV and PCLV, histone H4 affected the kinetics of DENV infection but was not essential for viral replication. Together, our data suggest that two highly prevalent ISVs, HTV and PCLV, affect mosquito vector competence for DENV and ZIKV by preventing the downregulation of histone H4, a novel proviral host factor. To test this hypothesis, we directly targeted histone H4 in mosquitoes carrying HTV and PCLV by using dsRNA-mediated gene silencing. We did not observe any changes in histone H4 expression in mosquitoes injected with cognate dsRNA (Extended Data Fig. 8h). This is in stark contrast to the efficient silencing triggered by the same dsRNA sequence in mosquitoes that did not carry HTV and PCLV (Extended Data Fig. 8g). Notably, another dsRNA targeting the AGO2 nuclease that is central to the RNA interference pathways was able to trigger efficient silencing in the same mosquitoes carrying HTV and PCLV (Extended Data Fig. 8i). These results again point to a specific effect of HTV and PCLV on histone H4 expression in mosquitoes.

Discussion

We report positive interactions between ISVs and arboviruses in mosquitoes in the wild and in the laboratory. Previously, ISVs have mainly been reported to interfere with arbovirus replication in mosquitoes (superinfection exclusion)^{7,31,32}. As HTV and PCLV are the most abundant ISVs that we detected in wild *A. aegypti* mosquitoes, it is feasible that they can have a substantial impact on the global transmission of DENV and ZIKV.

We also showed that HTV and PCLV increase histone H4 expression during DENV infection and that histone H4 is a proviral host factor for the replication of DENV in mosquitoes. We propose that ISVs increase DENV infection through upregulation of histone H4. However, we were unable to establish a direct connection between the regulation of histone H4 expression and the increase in vector competence. Regarding the role of histone H4 as a putative proviral factor, it is worth mentioning that C protein from flaviviruses interacts with histones and is capable of interfering with nucleosome assembly³³. Recent work further suggests that the C protein of yellow fever virus and possibly other flaviviruses mimics the tail of histone H4 and regulates gene expression to favour infection³⁴. Thus, downregulation of histone H4 may be part of a coordinated host response to limit the ability of flaviviruses to control gene expression, which could be counteracted by HTV and PCLV. We observed no major changes in gene expression in the presence of HTV and PCLV, which suggests that the proviral role of histone H4 is not achieved through major regulation of gene expression. Rather, replication-dependent histones seem to be preferentially regulated by HTV and PCLV, which could point to a mechanism involving cell division. Notably, replication-dependent histones are targeted by RNA

interference³⁵, which could provide a connection with the role of this pathway in the antiviral defence of mosquitoes^{16,36}.

Although previous studies have reported interactions between ISVs and arboviruses, most were performed in cell lines^{37–40}. Exceptions are the Nhumirim virus (NHUV) and the cell fusing agent virus (CFAV), which were shown to interfere with replication of arboviruses in the same family as West Nile virus, DENV and ZIKV^{31,41,42}. Interestingly, in cell lines, PCLV either inhibited or did not affect the replication of ZIKV^{21,22}. Also since we could not test the presence of PCLV alone in adult mosquitoes, we cannot rule out that HTV may have the predominant proviral effect.

Further work will be needed to understand how HTV and PCLV regulate histone H4 during DENV and ZIKV infection, and whether this mechanism affects other arboviruses such as CHIKV. Understanding how ISVs affect vector competence could reveal alternative strategies for controlling arbovirus transmission.

Methods

Ethics statement

All procedures involving vertebrate animals were approved by the ethical review committee of the Universidade Federal de Minas Gerais (CEUA 337/2016 and 118/2022 to J.T.M.). Mosquitoes were collected in Gabon under the research authorization AR0013/17/MESRS/CENAREST/CG/CST/CSAR delivered by CENAREST. Unlinked anonymous testing of human blood samples was approved by the ethics committee in research (COEP) of Universidade Federal de Minas Gerais (number 415/04 to E.G.K.).

Human blood samples

Human samples analysed in this study were collected and reported previously²⁰. Forty-four blood samples were collected from patients that sought medical attention in the city of Caratinga between February and July 2011 by professional nurses as part of a city surveillance plan. Blood samples were mixed with EDTA as an anticoagulant and stored at 4 °C. Serum was obtained from blood samples and inactivated at 56 °C for 30 min. Total RNA extraction from human blood samples was performed using TRIzol LS reagent (Invitrogen).

Data reporting

No statistical methods were used to predetermine sample size. Experiments were not randomized and investigators were not blinded to allocation during experiments and outcome assessment.

Mosquito collection in the field

Locations of mosquito collections are described in the Supplementary Table 1. Field traps were used to collect adult mosquitoes that were further identified using morphological characteristics. Whole mosquitoes were ground in TRIzol (Invitrogen) and kept refrigerated before RNA extraction. Collection and processing of individual mosquitoes from

Caratinga for spatiotemporal analysis of virus circulation were previously reported²⁰. RNA samples of these mosquitoes were re-analysed in this work.

RNA extraction

RNA was isolated using TRIzol reagent (Invitrogen) following the manufacturer's protocol with minor modifications. Briefly, individual mosquito samples or tissues were collected in 1.5 ml tubes; 3–5 glass beads (1 mm diameter) and ice-cold TRIzol were added before homogenization in a Mini-BeadBeater-16 (Biospec) for 90 s. Glycogen (Ambion) was added (10 µg per sample) to facilitate pellet visualization upon RNA precipitation. RNAs were resuspended in RNase-free water (Ambion) and stored at –80 °C.

Small RNA library construction

Different strategies for library construction were implemented and are indicated in Supplementary Table 1. The strategy was determined according to RNA quality evaluated by a 2100 Bioanalyzer system (Agilent). Libraries were built using total RNA or size-selected small RNAs (18–30 nt), depending on quality and yield of the sample. In the case of low RNA yield, especially when the source was a single mosquito, total RNA was directly used as input for library preparation. For samples with more than 20 µg of RNA available, small RNAs were selected by size (18–30 nt) on a denaturing PAGE. For samples with more than 20 µg of total RNA that displayed a degradation profile (that is, lack of sharp ribosomal RNA peaks), total RNA was subjected to oxidation using sodium periodate^{43,44} before size selection. Oxidized and non-oxidized size-selected RNAs (18–30 nt) were used as input for library construction. In all cases, libraries were prepared utilizing the TruSeq Small RNA Library prep kit (Illumina) or NEBNext Multiplex Small RNA Library prep set for Illumina (New England BioLabs) following protocols recommended by the manufacturers. Libraries were pooled and sequenced at the GenomEast sequencing platform at the Institut de Génétique et de Biologie Moléculaire et Cellulaire in Strasbourg, France.

Small RNA-based metagenomics for virus identification

After sequencing, raw sequenced reads from small RNA libraries were submitted to adaptor trimming using cutadapt⁴⁵ v1.12, discarding sequences with low Phred quality (<20), ambiguous nucleotides and/or with length shorter than 15 nt. Remaining sequences were mapped to reference sequences of *A. aegypti* (AaeL5)⁴⁶ or *A. albopictus*⁴⁷ using Bowtie⁴⁸ v1.1.2 allowing no mismatches. Size profiles of small RNAs matching reference sequences and 5' nt frequency were calculated using in-house Perl v5.16.3, BioPerl library v1.6.924 and R v3.3.1 scripts. Plots were made in R using ggplot2 v2.2.0 package. Sequences that did not present similarities with bacteria or the host genomes were used for contig assembly and subsequent analyses. Assembly was performed essentially as previously described⁸ with the following changes: (1) We replaced Velvet⁴⁹ assembler by SPAdes⁵⁰ on the second round of contig assembly. (2) Assembled contigs ranging from 50 to 199 nt were characterized solely on the basis of sequence similarity search against Viral RefSeq Database⁵¹. (3) Contigs greater than 200 nt were characterized on the basis of sequence similarity against the NCBI NT and NR databases and submitted to pattern-based strategies. (4) For manual curation of putative viral contigs, top 5 BLAST⁵² hits were analysed to rule out similarity to other organisms; Open reading frame (ORF) organization and small RNA size profile (distribution and coverage) were analysed to differentiate between viruses. Contigs containing truncated ORFs and small RNA profiles without the presence of symmetric small RNA peaks at 21 nt were considered to be endogenous viral elements (EVEs) as described¹⁵. (5) Manually curated viral contigs were grouped using CD-HIT⁵³ requiring 90% of coverage with 90% of identity to remove redundancy. Representative contigs were used for co-occurrence analysis based on small RNA abundance on each of the small RNA libraries available. Contigs grouped into a single cluster

(hierarchical clustering based on Pearson correlation) were then used as trusted on SPAdes for a re-assembly step using all the libraries in which that viral sequence was found. In total, we assembled 7,260 contigs larger than 200 nt (Fig. 1b, assembly metrics in Supplementary Table 2). Of 7,240 contigs, 1,448 were identified as putative viral sequences using sequence similarity searches against non-redundant nucleotide and protein databases (NT and NR databases, respectively) at GenBank (Fig. 1b and Supplementary Table 3). Although the number of contigs assembled per library varied greatly, we observed high abundance and diversity of viral contigs in most samples (Fig. 1c). Comparing results from the two mosquito species, the percentage of viral contigs was substantially smaller in *A. albopictus* libraries compared with *A. aegypti* (Fig. 1c). In addition, we noted more variation in the number of assembled contigs and larger proportions of unknown contigs in libraries from *A. albopictus*, probably because this species is less studied compared with *A. aegypti* (Fig. 1c). Most animal genomes contain integrated viral sequences known as EVEs that are transcribed and generate small RNAs^{54–56}. To discriminate sequences of viruses from EVEs, we took advantage of the small RNA profile associated with ORF analysis and contig size (Fig. 2a)¹⁵. This filter identified 446 putative EVE sequences that were removed from the initial viral contigs (Fig. 2a). The remaining viral contigs, representing putative viruses, were grouped into 158 unique clusters (on the basis of sequence similarity) (Supplementary Table 4). In 19 clusters, parts of contigs had significant similarity to two different viruses. Our results suggested that these were misassemblies and they were thus removed from further analyses (Fig. 2a). Contigs representing the remaining clusters were used to evaluate co-occurrence in the 91 small RNA libraries from *A. aegypti* and *A. albopictus* (Extended Data Fig. 1). The occurrence of contigs in each library was indicated by the normalized number of small RNA reads mapped to each reference. Across the small RNA libraries, contigs that consistently co-occurred and shared similar expression profiles were considered probable fragments from the same viral genome (Fig. 2a). This analysis yielded a total of 12 clusters of co-occurring contigs and 3 single contigs that had no additional partners. Contigs from each cluster were further analysed on the basis of the closest reference sequence to determine the putative organization of fragments along the viral genome. This analysis showed that clusters 2 and 3 contained contigs belonging to the same virus, PCLV, and were considered together for further analyses (Extended Data Fig. 1). To further classify the clusters and single contigs, we focused on the ones that represented sequences encoding viral polymerases. We were able to identify clear polymerase sequences in each of the 11 clusters and in 1 out of the 3 single contigs.

Phylogenetic analyses

Assembled viral contigs were submitted to analysis of conserved domains to identify RNA dependent RNA polymerase (RdRp)-related regions using NCBI Conserved Domain Search (<https://www.ncbi.nlm.nih.gov/Structure/cdd/wrpsb.cgi>). For each putative virus, the largest RdRp segment was used to identify virus relatives at NCBI sequence databases (NT and NR) using sequence-similarity searches through the BLAST tool. Multiple alignments were performed using the MAFFT online tool⁵⁷ available at <https://www.ebi.ac.uk/Tools/msa/mafft/>. For putative new viruses identified at protein level (*Narnaviridae*, *Partitiviridae*, *Rhabdoviridae*, *Totiviridae* and *Virgaviridae*), amino acid sequences were selected, and phylogenetic analyses were carried out on CIPRES Portal version 3.3 (<https://www.phylo.org/portal2>)⁵⁸. The best-fit model of protein evolution was selected in ModelTest-NG⁵⁹ for each viral species, using the maximum-likelihood method. For the virus from *Totiviridae* family, an additional strategy was also applied using nucleotide sequences where the best-fit model was defined using MEGA-X tool⁶⁰, and the tree was constructed using the maximum-likelihood method. For all phylogenetic trees, clade robustness was assessed using the bootstrap method (1,000 pseudoreplicates) and trees were edited using iTOL version 5.7⁶¹ (<https://itol.embl.de/>).

Mosquitoes

Wild *A. aegypti* mosquitoes used in cage experiments were F₂ to F₅ generations derived from eggs collected in Rio de Janeiro (Urca neighbourhood) in Brazil and were kindly provided by Dr Rafael M. de Freitas from Fiocruz-RJ and Dr Luciano A. Moreira from Fiocruz-MG. The laboratory Red-eye strain⁶² was kindly provided by Prof. Pedro C. Oliveira from the Universidade Federal do Rio de Janeiro - UFRJ. *A. aegypti* mosquitoes were maintained in a climatic chamber at 28 °C and 70–80% relative humidity in a 14:10 h light:dark photoperiod, with 10% sucrose solution provided ad libitum. Mosquito cages contained individuals that emerged in a 48 h interval.

Generation of HTV+/PCLV+ and HTV-/PCLV- mosquito lines

Mosquito lines persistently infected with PCLV and HTV or non-infected counterparts were generated from F₂ generations of wild mosquitoes. Three days after a blood meal, F₂ mated females were individually isolated in tubes containing a filter paper and 0.5 cm of water, and were allowed to lay eggs for 24 h. Individual females were collected, and the total RNA was isolated using TRIzol (Invitrogen) following the standard protocol. Detection of HTV and PCLV was performed by RT-qPCR using the primers described in Supplementary Table 5. Eggs corresponding to 5 female mosquitoes infected with HTV, PCLV or both viruses were pooled before hatching. Pools of eggs from 5 females negative for both viruses were similarly pooled to create virus-free lines. Subsequent detection of HTV and PCLV was performed to confirm correct identification of lines. Lines generated from females carrying a single virus (HTV or PCLV) were tested and found to carry both viruses. Therefore, only virus-free and double infected lines were expanded for two more generations for experiments described in this work.

Artificial infection of naïve laboratory *A. aegypti* mosquitoes with HTV and PCLV

Extracts of naturally infected *A. aegypti* mosquitoes were used as source for HTV and PCLV since we were not able to produce these viruses in cell culture. Viral stocks were produced from pools of 15 *A. aegypti* naturally infected with HTV and PCLV or non-infected mosquitoes (virus-free controls) that were ground using pestles in 1,200 µl of L-15 Leibovitz medium (Gibco) supplemented with 10% fetal bovine serum (FBS). Samples were centrifuged at 3,000 × *g* for 15 min at 4 °C for clarification. Supernatants were collected and passed through a 0.22 µm filter, aliquoted and stored at –80 °C before use. Infection with HTV and PCLV or mock control was performed by microinjecting 69 nl of the extract into naïve laboratory mosquitoes (*A. aegypti* Red-Eye strain) using a Nanoject II microinjector (Drummond).

Infection of Vero cells with HTV and PCLV

Filtered *A. aegypti* extracts (500 µl) containing HTV and PCLV (obtained as described above) were transferred into T-25 flasks containing 90% confluent Vero cells in non-supplemented DMEM medium. After 1 h of viral adsorption, 4.5 ml of DMEM medium supplemented with penicillin/streptomycin and 10% FBS were added to cells that were incubated at 37 °C and 5% CO₂. Aliquots (100 µl) of the supernatant were collected during each passage on days 1, 3 and 5 after exposure to HTV and PCLV. Virus in the supernatant was assessed by RT-qPCR. Vesicular stomatitis virus was added as a spike immediately before RNA extraction for use as an internal control.

DENV and ZIKV propagation

Viral isolates of DENV1 (MV09) and ZIKV (PE243/2015)⁶³ were propagated in C6/36 *A. albopictus* cells or Vero cells, respectively. For DENV1 propagation, C6/36 cells were maintained on L-15 medium supplemented with 5% FBS and 1× antibiotic-antimycotic (Gibco) as previously described²⁰. Cells were seeded to 70% confluence, infected at a multiplicity of infection of 0.01 and maintained for 6–9 d at 28 °C. For ZIKV propagation, a similar procedure was followed using Vero cells

that were maintained in DMEM medium supplemented with 10% FBS and 1× antibiotic-antimycotic (Gibco). Vero cells were seeded to a confluence of 70–80%, infected with ZIKV at a multiplicity of infection of 0.01 and maintained in culture for 6 d. For both viruses, the supernatant was collected and clarified by centrifugation to generate virus stocks that were kept at –80 °C before use. Mock-infected supernatants used as controls were prepared under the same procedure without virus infection. Titration of DENV1 was performed in BHK-21 cells, while ZIKV was titrated in Vero cells, both using the plaque assay method to determine viral titre.

DENV and ZIKV infection in mosquitoes

Natural infection in mosquitoes was performed using mice deficient in interferon-I and interferon-II receptors as previously described¹⁹. Briefly, infection in AG129 mice was established by intraperitoneal injection of approximately 10⁶ plaque forming units (p.f.u.) of DENV1 or 10⁶ p.f.u. of ZIKV. Infected mice were anaesthetized at 3 d.p.i. (peak of viraemia) using ketamine/xylazine (80/8 mg kg⁻¹) and placed on top of the netting-covered containers with adult mosquito females. Mosquitoes were allowed to feed on mice for 30 min to 1 h, alternating on the same animal between cages every 10 min if two groups were to be compared. Viremia of each mouse was tested by RT-qPCR immediately after feeding and the experiment would be discarded if a discrepancy in viral load of more than 10× was observed. For infections by membrane feeding, 5–6-day-old adult females were starved for 24 h and fed with a mixture of blood and virus supernatant containing 10⁷ p.f.u. ml⁻¹ of DENV serotype 1, utilizing a glass artificial feeding system covered with pig intestine membrane as previously described¹⁹. After blood feeding, fully engorged females were selected and kept in standard rearing conditions until collection at different time points. Mosquitoes infected by injection were anaesthetized by being placed in a fridge at 4 °C and kept on ice during the whole procedure. Virus stocks were diluted with L-15 medium (Gibco) and injections were carried out using the Nanoject II microinjector (Drummond) with a volume of 69 nl. Each individual mosquito was injected with 16 p.f.u. of DENV or ZIKV. Mosquitoes were collected at different days post injection for dissection and RNA extraction. Tissues (midguts, salivary glands and ovaries) were dissected in ice-cold 1× phosphate buffered saline (PBS) containing 0.01% Triton X-100 (Sigma). Remnants of mosquito tissues were considered as carcass, as illustrated in figure schemes. Tissues or mosquitoes were ground in TRIzol (Invitrogen) using glass beads as previously described¹⁹ and kept frozen at –80 °C until RNA extraction as described above.

Mouse model for vectorial transmission of arboviruses

Groups of mosquitoes naturally infected with HTV and PCLV or PCLV/HTV-free siblings were fed on the same ZIKV-infected AG129 mouse as described above. One mouse was used per time point of transmission that was evaluated. Engorged females were kept after feeding and, 3 d later, allowed to lay eggs for 48 h in dark cups containing 1 cm of water and a paper sheet attached to their walls. At 6, 8 and 12 d.p.f., 10–12 mosquito females of each group were allowed to feed on naïve AG129 mice for up to 3 h. Mice were bled 3 d after mosquito biting and viral RNA levels were quantified by RT-qPCR. Viral loads were also quantified by RT-qPCR in engorged mosquitoes from each group after feeding on a naïve mouse.

dsRNA-mediated gene silencing

RNA transcription was performed using T7 Megascript kit (Ambion) following the manufacturer's instructions. Briefly, template DNA containing T7 promoter sequences in both 5' and 3' extremities was obtained by RT-PCR for dsAGO2 and dsH4, or by PCR amplification from plasmid pDSAG (Addgene 62289) for dsGFP. Primer sequences are provided in Supplementary Table 5. Adult 4-day-old females were intrathoracically injected with 69 nl of a dsRNA solution (7.2 µg µl⁻¹) diluted in

annealing buffer (20 mM Tris-HCl pH 7.5, 100 mM NaCl) using a Nanoject II nano-injector (Drummond). Mosquitoes were allowed to recover for 48 h before further experiments. Once recovered, dsRNA-injected mosquitoes were allowed to feed or were microinjected with virus following the procedures described above.

RT-qPCR and RT-PCR

Total RNA extracted from individual mosquitoes or individual tissues were reverse transcribed using M-MLV reverse transcriptase (RT), utilizing random primers (hexamers) for initiation. Negative controls were prepared following the same protocol without adding reverse transcriptase. Complementary DNA was subjected to polymerase chain reaction (RT-PCR) using the GoTaq Hot Start Green PCR master mix (Promega) or quantitative polymerase chain reaction (RT-qPCR) utilizing the Power SYBR Green master mix (Applied Biosystems) following manufacturer instructions. Results were expressed using the $2^{-\Delta Ct}$ method relative to the endogenous control *rpl32*. Primer sequences are listed in Supplementary Table 5. In experiments designed to differentiate the expression of histone H4 polyA transcripts versus non-polyA transcripts, cDNAs were synthesized starting from the same amount of total RNA in two independent reactions using either random hexamers or anchored oligo dT₂₂ as reverse transcription initiators. Subsequent quantifications by RT-qPCR were performed as described above.

Mathematical model

To investigate the effect of variations in the EIP on the cumulative incidence of DENV infections, we used a previously developed spatially explicit, individual-based meta-population model²⁸. Briefly, humans and mosquitoes are defined with a unique state representing their current epidemiological status and, in the case of humans, their infection history. Human individuals are considered to be either susceptible, exposed, infectious or recovered with respect to each serotype, allowing up to four sequential infections. For mosquitoes, only the susceptible, exposed and infectious states of the epidemiologically relevant adult life-stage are considered. The sizes of the respective populations are kept constant, with deaths being replaced by births. For simplicity, rather than accounting for seasonality through changes in mosquito densities or temperature-dependent variations in EIP, this is done here by varying daily mosquito biting rates (a_v), given as

$$a_v(t) = a_0 \left(\beta + (1 - \beta) \sin(\pi t / 364) \right)^4,$$

where t denotes time in days, a_0 the vector biting rate, β the seasonality factor, and assuming a year of 364 days. Both human and vector mortality rates are age-dependent, that is, the per capita risk of death is assumed to increase with age, which prevents individuals from living beyond biologically reasonable ages. For computational efficiency, individuals' life expectancies are assigned at birth. Spatial structure is included by subdividing humans and mosquitoes into spatially organized sets of non-overlapping communities, where individuals mix homogeneously. Mosquitoes preferentially bite humans in their own community and adjacent communities but can also bite individuals of non-adjacent communities with low probability to account for (daily) human mobility and associated long-distance transmission events. Parameter values are listed in Supplementary Table 6 and were chosen to capture the qualitative dynamics of DENV in a high-transmission setting with four co-circulating serotypes (DENV1-4).

The model exhibits pronounced demographic and epidemiological stochasticities that arise from the fully probabilistic nature of state transitions and result in significant inter-annual oscillations in both disease incidence and relative prevalence of the four co-circulating serotypes. To investigate the effect of shortening or extending the EIP, we ran the model for a period of 100 yr and recorded the total annual number of infections for the last 50 yr, discarding the transient dynamics. Due to the stochastic nature of the model, we averaged the 50 yr

cumulative incidence over five model runs for each value of the EIP. Mosquito and human prevalence were equally evaluated over a 50 yr time period but taken as the proportion of infected individuals on a single day during the seasonal peak, resulting in 50 individual data points.

PolyA selection, RNA library construction and transcriptomic analysis

RNA samples from individual mosquitoes were pooled and RNA quality was verified using the 2100 Bioanalyzer system (Agilent). mRNA libraries were constructed using the NEBNext Poly(A) mRNA magnetic isolation module and NEBNext Ultra II Directional RNA Library prep kit for Illumina (New England BioLabs) following the manufacturers' protocol. Libraries were pooled and sequenced at the GenomEast sequencing platform at the Institut de Génétique et de Biologie Moléculaire et Cellulaire in Strasbourg, France. Sequenced reads with an average quality score above phred 25 had adaptors removed using Trimmomatic v0.39 and were further mapped to the decoyed transcriptome of *A. aegypti* (Vectorbase release 48) using Salmon v1.3.0^{64,65}. Quasi-mapping quantifications were imported into R v3.6.3 and data normalization was performed using the packages EdgeR v3.28.1 and TMM^{66,67}. Differentially expressed genes were inferred using the exactTest function (assigning a square-root-dispersion of 0.4) whose input was used in the function decideTestsDGE. Fold-change plots were created using the package ggplot2 v3.3.6 and Euler diagrams generated with the package venneuler v1.1-3. Heat maps were generated using the R packages tydiverse v1.3.1 and gplots v3.1.3. Ranked lists of gene expression for each comparison were used as input for GSEA²⁸ using the R package fgsea v1.12.0⁶⁸ and in-house-developed gene sets comprising gene ontology annotation, pathways and genes of interest. Sets with adjusted $P < 0.1$ were considered in our analysis.

Analysis of histone H4 genes in *A. aegypti*

Alignment of putative *histone H4* genes was performed using the T-Coffee webserver⁶⁹ with the variant M-Coffee that allows combining multiple outputs from different aligners (MAFFT, Clustal and Muscle). The model (TN93 + I) for the phylogenetic reconstruction was defined using SMS within the PhyML server^{70,71}. Finally, the maximum-likelihood tree was constructed with PhyML requiring 1,000 bootstrap replicates and edited using the iTOL server⁶¹. The *histone H4* polyadenylation signature was defined according to the presence of a canonical polyadenylation signal (AAUAAA) as previously described³⁵. The *histone H4* expression heat map shown in Extended Data Fig. 8d was produced in R v4.0.2 using the package gplots v3.1.3 and shows transcript per million (TPM) counts normalized by Z-score (row) and sorted according to the phylogenetic tree. Libraries were obtained at the Sequence Read Archive (SRA/NCBI) and accession numbers are shown.

Statistical analyses

Evaluation of statistical significance was performed using GraphPad Prism 9.0 or R-cran v3.3.1 software unless stated otherwise. Viral loads of RT-qPCR positive-only individual mosquito/tissues were log transformed and subjected to Mann-Whitney U -test. Pairwise comparisons of virus infection prevalence were evaluated using Fisher's exact test or sequentially by a generalized linear model considering the interaction between time points and their prevalence, followed by type II analysis of variance (ANOVA) using the car package v3.1-0 in R. Presence and absence of DENV in mosquitoes was modelled with univariate and multivariate zero-inflated binomial model^{72,73} since 95% of the collections are zeroes. The covariate or covariates (in the case of the multivariate model) was/were the same for the logit and logistic parts of the model. In particular, we considered PCLV, HTV and their interaction. Model selection was carried out using Akaike's information criterion (AIC) and Bayesian information criterion (BIC) comparison⁷⁴. The Vuong test was conducted a priori to test whether the zero-inflated binomial model was statistically significant and better (in terms of AIC and BIC)

than a non-zero-inflated model. Data were analysed using R and the ‘pscl’ package v1.5.5²⁵. Finally, we tested the presence of spatial autocorrelation in the two viruses via variogram analyses²⁰, but no significant autocorrelations were found (results not reported).

Reporting summary

Further information on research design is available in the Nature Portfolio Reporting Summary linked to this article.

Data availability

Small RNA and transcriptome libraries from this study have been deposited in the Sequence Read Archive (SRA) at NCBI (project accession [PRJNA722589](https://www.ncbi.nlm.nih.gov/submit/sra/?term=PRJNA722589)). Sequences spanning the RdRP region from newly discovered viruses were deposited in GenBank under accession MZ556103-MZ556111. Accession numbers for small RNA libraries are provided in Supplementary Table 1. Source data are provided with this paper.

Code availability

All scripts used in this work were deposited in GitHub and can be accessed at <https://github.com/ericgdp/sRNA-virome> code version 1.0.

References

- Weaver, S. C., Charlier, C., Vasilakis, N. & Lecuit, M. Zika, chikungunya, and other emerging vector-borne viral diseases. *Annu. Rev. Med.* **69**, 395–408 (2018).
- Bhatt, S. et al. The global distribution and burden of dengue. *Nature* **496**, 504–507 (2013).
- Messina, J. P. et al. Global spread of dengue virus types: mapping the 70 year history. *Trends Microbiol.* **22**, 138–146 (2014).
- Franklinos, L. H. V., Jones, K. E., Redding, D. W. & Abubakar, I. The effect of global change on mosquito-borne disease. *Lancet Infect. Dis.* **19**, e302–e312 (2019).
- Kraemer, M. U. G. et al. Past and future spread of the arbovirus vectors *Aedes aegypti* and *Aedes albopictus*. *Nat. Microbiol.* **4**, 854–863 (2019).
- Cromwell, E. A. et al. The relationship between entomological indicators of *Aedes aegypti* abundance and dengue virus infection. *PLoS Negl. Trop. Dis.* **11**, e0005429 (2017).
- de Almeida, J. P., Aguiar, E. R., Armache, J. N., Olmo, R. P. & Marques, J. T. The virome of vector mosquitoes. *Curr. Opin. Virol.* **49**, 7–12 (2021).
- Aguiar, E. R. G. R. et al. Sequence-independent characterization of viruses based on the pattern of viral small RNAs produced by the host. *Nucleic Acids Res.* **43**, 6191–6206 (2015).
- Boyles, S. M. et al. Under-the-radar dengue virus infections in natural populations of *Aedes aegypti* mosquitoes. *mSphere* **5**, e00316–20 (2020).
- Ramos-Nino, M. E. et al. High prevalence of Phasi Charoen-like virus from wild-caught *Aedes aegypti* in Grenada, W.I. as revealed by metagenomic analysis. *PLoS ONE* **15**, e0227998 (2020).
- Shi, C. et al. Stable distinct core eukaryotic viromes in different mosquito species from Guadeloupe, using single mosquito viral metagenomics. *Microbiome* **7**, 121 (2019).
- Zakrzewski, M. et al. Mapping the virome in wild-caught *Aedes aegypti* from Cairns and Bangkok. *Sci. Rep.* **8**, 4690 (2018).
- Patterson, E. I., Villinger, J., Muthoni, J. N., Dobel-Ober, L. & Hughes, G. L. Exploiting insect-specific viruses as a novel strategy to control vector-borne disease. *Curr. Opin. Insect Sci.* **39**, 50–56 (2020).
- Vasilakis, N. & Tesh, R. B. Insect-specific viruses and their potential impact on arbovirus transmission. *Curr. Opin. Virol.* **15**, 69–74 (2015).
- Aguiar, E. R. G. R., Olmo, R. P. & Marques, J. T. Virus-derived small RNAs: molecular footprints of host-pathogen interactions. *Wiley Interdiscip. Rev. RNA* **7**, 824–837 (2016).
- Morazzani, E. M., Wiley, M. R., Murreddu, M. G., Adelman, Z. N. & Myles, K. M. Production of virus-derived ping-pong-dependent piRNA-like small RNAs in the mosquito soma. *PLoS Pathog.* **8**, e1002470 (2012).
- Myles, K. M., Wiley, M. R., Morazzani, E. M. & Adelman, Z. N. Alphavirus-derived small RNAs modulate pathogenesis in disease vector mosquitoes. *Proc. Natl Acad. Sci. USA* **105**, 19938–19943 (2008).
- Frangeul, L., Blanc, H., Saleh, M.-C. & Suzuki, Y. Differential small RNA responses against co-infecting insect-specific viruses in *Aedes albopictus* mosquitoes. *Viruses* **12**, 468 (2020).
- Olmo, R. P. et al. Control of dengue virus in the midgut of *Aedes aegypti* by ectopic expression of the dsRNA-binding protein Loqs2. *Nat. Microbiol.* **3**, 1385–1393 (2018).
- Sedda, L. et al. The spatial and temporal scales of local dengue virus transmission in natural settings: a retrospective analysis. *Parasit. Vectors* **11**, 79 (2018).
- Schultz, M. J., Frydman, H. M. & Connor, J. H. Dual insect specific virus infection limits Arbovirus replication in *Aedes* mosquito cells. *Virology* **518**, 406–413 (2018).
- Fredericks, A. C. et al. *Aedes aegypti* (Aag2)-derived clonal mosquito cell lines reveal the effects of pre-existing persistent infection with the insect-specific bunyavirus Phasi Charoen-like virus on arbovirus replication. *PLoS Negl. Trop. Dis.* **13**, e0007346 (2019).
- Sedda, L., Taylor, B. M., Eiras, A. E., Marques, J. T. & Dillon, R. J. Using the intrinsic growth rate of the mosquito population improves spatio-temporal dengue risk estimation. *Acta Trop.* **208**, 105519 (2020).
- Lin, J.-J. et al. Aggressive organ penetration and high vector transmissibility of epidemic dengue virus-2 cosmopolitan genotype in a transmission mouse model. *PLoS Pathog.* **17**, e1009480 (2021).
- Sun, P. et al. A mosquito salivary protein promotes flavivirus transmission by activation of autophagy. *Nat. Commun.* **11**, 260 (2020).
- Lourenço, J. & Recker, M. Natural, persistent oscillations in a spatial multi-strain disease system with application to dengue. *PLoS Comput. Biol.* **9**, e1003308 (2013).
- Lourenço, J. et al. Epidemiological and ecological determinants of Zika virus transmission in an urban setting. *eLife* **6**, e29820 (2017).
- Subramanian, A. et al. Gene set enrichment analysis: a knowledge-based approach for interpreting genome-wide expression profiles. *Proc. Natl Acad. Sci. USA* **102**, 15545–15550 (2005).
- Flaus, A., Downs, J. A. & Owen-Hughes, T. Histone isoforms and the oncohistone code. *Curr. Opin. Genet. Dev.* **67**, 61–66 (2021).
- Lyons, S. M. et al. A subset of replication-dependent histone mRNAs are expressed as polyadenylated RNAs in terminally differentiated tissues. *Nucleic Acids Res.* **44**, 9190–9205 (2016).
- Baidaliuk, A. et al. Cell-fusing agent virus reduces arbovirus dissemination in *Aedes aegypti* mosquitoes in vivo. *J. Virol.* **93**, e00705–e00719 (2019).
- Blitvich, B. J. & Firth, A. E. Insect-specific flaviviruses: a systematic review of their discovery, host range, mode of transmission, superinfection exclusion potential and genomic organization. *Viruses* **7**, 1927–1959 (2015).
- Colpitts, T. M., Barthel, S., Wang, P. & Fikrig, E. Dengue virus capsid protein binds core histones and inhibits nucleosome formation in human liver cells. *PLoS ONE* **6**, e24365 (2011).
- Mourão, D. et al. A histone-like motif in yellow fever virus contributes to viral replication. Preprint at *bioRxiv* <https://doi.org/10.1101/2020.05.05.078782> (2020).

35. Girardi, E. et al. Histone-derived piRNA biogenesis depends on the ping-pong partners Piwi5 and Ago3 in *Aedes aegypti*. *Nucleic Acids Res.* **45**, 4881–4892 (2017).
36. Varjak, M. et al. *Aedes aegypti* Piwi4 is a noncanonical PIWI protein involved in antiviral responses. *mSphere* **2**, e00144-17 (2017).
37. Parry, R. & Asgari, S. *Aedes anophevirus*: an insect-specific virus distributed worldwide in *Aedes aegypti* mosquitoes that has complex interplays with *Wolbachia* and dengue virus infection in cells. *J. Virol.* **92**, e00224-18 (2018).
38. Zhang, G., Asad, S., Khromykh, A. A. & Asgari, S. Cell fusing agent virus and dengue virus mutually interact in *Aedes aegypti* cell lines. *Sci. Rep.* **7**, 6935 (2017).
39. Nasar, F., Erasmus, J. H., Haddow, A. D., Tesh, R. B. & Weaver, S. C. Eilat virus induces both homologous and heterologous interference. *Virology* **484**, 51–58 (2015).
40. Kenney, J. L., Solberg, O. D., Langevin, S. A. & Brault, A. C. Characterization of a novel insect-specific flavivirus from Brazil: potential for inhibition of infection of arthropod cells with medically important flaviviruses. *J. Gen. Virol.* **95**, 2796–2808 (2014).
41. Romo, H., Kenney, J. L., Blitvich, B. J. & Brault, A. C. Restriction of Zika virus infection and transmission in *Aedes aegypti* mediated by an insect-specific flavivirus. *Emerg. Microbes Infect.* **7**, 1–13 (2018).
42. Goenaga, S. et al. Potential for co-infection of a mosquito-specific flavivirus, nhumirim virus, to block West Nile virus transmission in mosquitoes. *Viruses* **7**, 5801–5812 (2015).
43. Alefelder, S., Patel, B. K. & Eckstein, F. Incorporation of terminal phosphorothioates into oligonucleotides. *Nucleic Acids Res.* **26**, 4983–4988 (1998).
44. Marques, J. T. et al. Loqs and R2D2 act sequentially in the siRNA pathway in *Drosophila*. *Nat. Struct. Mol. Biol.* **17**, 24–30 (2010).
45. Martin, M. Cutadapt removes adapter sequences from high-throughput sequencing reads. *EMBnet j.* **17**, 10–12 (2011).
46. Matthews, B. J. et al. Improved reference genome of *Aedes aegypti* informs arbovirus vector control. *Nature* **563**, 501–507 (2018).
47. Chen, X.-G. et al. Genome sequence of the Asian Tiger mosquito, *Aedes albopictus*, reveals insights into its biology, genetics, and evolution. *Proc. Natl Acad. Sci. USA* **112**, E5907–E5915 (2015).
48. Langmead, B., Trapnell, C., Pop, M. & Salzberg, S. L. Ultrafast and memory-efficient alignment of short DNA sequences to the human genome. *Genome Biol.* **10**, R25 (2009).
49. Zerbino, D. R. Using the Velvet de novo assembler for short-read sequencing technologies. *Curr. Protoc. Bioinform.* <https://doi.org/10.1002/0471250953.bi1105s31> (2010).
50. Bankevich, A. et al. SPAdes: a new genome assembly algorithm and its applications to single-cell sequencing. *J. Comput. Biol.* **19**, 455–477 (2012).
51. O’Leary, N. A. et al. Reference sequence (RefSeq) database at NCBI: current status, taxonomic expansion, and functional annotation. *Nucleic Acids Res.* **44**, D733–D745 (2016).
52. Altschul, S. F., Gish, W., Miller, W., Myers, E. W. & Lipman, D. J. Basic local alignment search tool. *J. Mol. Biol.* **215**, 403–410 (1990).
53. Fu, L., Niu, B., Zhu, Z., Wu, S. & Li, W. CD-HIT: accelerated for clustering the next-generation sequencing data. *Bioinformatics* **28**, 3150–3152 (2012).
54. Aguiar, E. R. G. R. et al. A single unidirectional piRNA cluster similar to the flamenco locus is the major source of EVE-derived transcription and small RNAs in *Aedes aegypti* mosquitoes. *RNA* **26**, 581–594 (2020).
55. Whitfield, Z. J. et al. The diversity, structure, and function of heritable adaptive immunity sequences in the *Aedes aegypti* genome. *Curr. Biol.* **27**, 3511–3519.e7 (2017).
56. Palatini, U. et al. Comparative genomics shows that viral integrations are abundant and express piRNAs in the arboviral vectors *Aedes aegypti* and *Aedes albopictus*. *BMC Genomics* **18**, 512 (2017).
57. Katoh, K., Misawa, K., Kuma, K. & Miyata, T. MAFFT: a novel method for rapid multiple sequence alignment based on fast Fourier transform. *Nucleic Acids Res.* **30**, 3059–3066 (2002).
58. Miller, M. A., Pfeiffer, W. & Schwartz, T. The CIPRES science gateway: a community resource for phylogenetic analyses. In *Towns J. Proc. 2011 TeraGrid Conference on Extreme Digital Discovery - TG '11* 41, 1–8 (ACM Press, 2011).
59. Darrriba, D. et al. ModelTest-NG: a new and scalable tool for the selection of DNA and protein evolutionary models. *Mol. Biol. Evol.* **37**, 291–294 (2020).
60. Kumar, S., Stecher, G., Li, M., Knyaz, C. & Tamura, K. MEGA X: molecular evolutionary genetics analysis across computing platforms. *Mol. Biol. Evol.* **35**, 1547–1549 (2018).
61. Letunic, I. & Bork, P. Interactive Tree Of Life (iTOL) v4: recent updates and new developments. *Nucleic Acids Res.* **47**, W256–W259 (2019).
62. Barletta, A. B. F. et al. Microbiota activates IMD pathway and limits Sindbis infection in *Aedes aegypti*. *Parasit. Vectors* **10**, 103 (2017).
63. Donald, C. L. et al. Full genome sequence and sfRNA interferon antagonist activity of Zika virus from Recife, Brazil. *PLoS Negl. Trop. Dis.* **10**, e0005048 (2016).
64. Bolger, A. M., Lohse, M. & Usadel, B. Trimmomatic: a flexible trimmer for Illumina sequence data. *Bioinformatics* **30**, 2114–2120 (2014).
65. Patro, R., Duggal, G., Love, M. I., Irizarry, R. A. & Kingsford, C. Salmon provides fast and bias-aware quantification of transcript expression. *Nat. Methods* **14**, 417–419 (2017).
66. Robinson, M. D. & Oshlack, A. A scaling normalization method for differential expression analysis of RNA-seq data. *Genome Biol.* **11**, R25 (2010).
67. Robinson, M. D., McCarthy, D. J. & Smyth, G. K. edgeR: a Bioconductor package for differential expression analysis of digital gene expression data. *Bioinformatics* **26**, 139–140 (2010).
68. Korotkevich, G. et al. Fast gene set enrichment analysis. Preprint at *bioRxiv* <https://doi.org/10.1101/060012> (2016).
69. Di Tommaso, P. et al. T-Coffee: a web server for the multiple sequence alignment of protein and RNA sequences using structural information and homology extension. *Nucleic Acids Res.* **39**, W13–W17 (2011).
70. Guindon, S. et al. New algorithms and methods to estimate maximum-likelihood phylogenies: assessing the performance of PhyML 3.0. *Syst. Biol.* **59**, 307–321 (2010).
71. Lefort, V., Longueville, J.-E. & Gascuel, O. SMS: Smart Model Selection in PhyML. *Mol. Biol. Evol.* **34**, 2422–2424 (2017).
72. Lambert, D. Zero-inflated Poisson regression, with an application to defects in manufacturing. *Technometrics* **34**, 1–14 (1992).
73. Hilbe, J. M. *Negative Binomial Regression* (2007).
74. Cameron, A. C. & Trivedi, P. K. *Regression Analysis of Count Data* (Cambridge Univ. Press, 1998).
75. Zeileis, A., Kleiber, C. & Jackman, S. Regression models for count data in R. *J. Stat. Softw.* **27**, 8 (2008).

Acknowledgements

We thank all members of the ZIKAlliance consortium, especially A.-B. Failloux and A. Kohl for helping with establishing a network of collaborators and contributing fruitful discussions; current and former members of the Marques laboratory and the M3i unit - Insect Models of Innate Immunity, especially S. Blandin and N. Martins for suggestions and discussions. This work of the Interdisciplinary Thematic Institute IMCBio, as part of the ITI 2021-2028 programme of the University of Strasbourg, CNRS and Inserm, was supported by IdEx Unistra (ANR-10-IDEX-0002), by the SFRI-STRAT'US project

(ANR 20-SFRI-0012), and EUR IMCBio (IMCBio ANR-17-EURE-0023) under the framework of the French Investments for the Future Program as well as by the previous Labex NetRNA (ANR-10-LABX-0036) to J.T.M. and J.-L.I. This work was also supported by grants from Conselho Nacional de Desenvolvimento Científico e Tecnológico (CNPq) to J.T.M. and E.R.G.R.A.; Fundação de Amparo a Pesquisa do Estado de Minas Gerais (FAPEMIG), Rede Mineira de Imunobiológicos (grant no. REDE-00140-16), Rede Mineira de Biomoléculas (grant no. REDE-00125-16), Instituto Nacional de Ciência e Tecnologia de Vacinas (INCTV), Fonds Régional de Coopération pour la Recherche FRCT2020 Région Grand-Est – ViroMod and Institute for Advanced Studies of the University of Strasbourg (USIAS fellowship 2019 to J.T.M.); Google Latin American Research Award (LARA 2019) to J.T.M. and J.P.P.d.A.; FAPESP (Grant No. 13/21719-3) to M.L.N.; the European Union's Horizon 2020 research and innovation programme under ZIKAlliance grant agreement no. 734548 and Investissement d'Avenir Programs (ANR-10-LABX-0036 and ANR-11-EQPX-0022) to J.-L.I. and J.T.M.; and ANR PRC TIGERBRIDGE, grant no. 16-CE35-0010-01 to C.P. J.T.M., B.P.D., E.G.K and M.L.N. are CNPq Research Fellows. M.L.N. was partly funded by the Centers for Research in Emerging Infectious Diseases (CREID), the Coordinating Research on Emerging Arboviral Threats Encompassing the Neotropics (CREATE-NEO) grant U01 AI151807 by the National Institutes of Health (NIH/USA). This study was financed in part by the Coordenação de Aperfeiçoamento de Pessoal de Nível Superior—Brasil (CAPES)—Finance Code 001 to J.T.M. and V.A.-S. R.P.O. received a post-doctoral fellowship from CAPES.

Author contributions

R.P.O., E.R.G.R.A., J.-L.I. and J.T.M. conceived the project. R.P.O., Y.M.H.T., E.R.G.R.A., J.P.P.d.A., J.N.A., L.S. and J.T.M. designed the experiments and performed computational analysis. R.P.O., Y.M.H.T., I.J.S.d.F., F.V.F., A.G.A.F., S.C.G.A., A.T.S.S., K.P.R.d.S., A.P.P.V. and A.B. performed experiments. C.H.T., M.D., A.G., C.P., J.O.-N., T.M.V., C.J.M.K., M.A.W., A.L.C.C., M.T.P., M.C.P.P., M.L.N., V.A.-S., R.N.M., M.A.Z.B., B.P.D., E.G.K. and E.M. provided samples and reagents. M.R. performed the mathematical

modelling. R.P.O., Y.M.H.T., E.R.G.R.A., J.-L.I. and J.T.M. wrote the manuscript. All authors read and contributed to manuscript editing.

Competing interests

The authors declare no competing interests.

Additional information

Extended data is available for this paper at <https://doi.org/10.1038/s41564-022-01289-4>.

Supplementary information The online version contains supplementary material available at <https://doi.org/10.1038/s41564-022-01289-4>.

Correspondence and requests for materials should be addressed to João T. Marques.

Peer review information *Nature Microbiology* thanks the anonymous reviewers for their contribution to the peer review of this work.

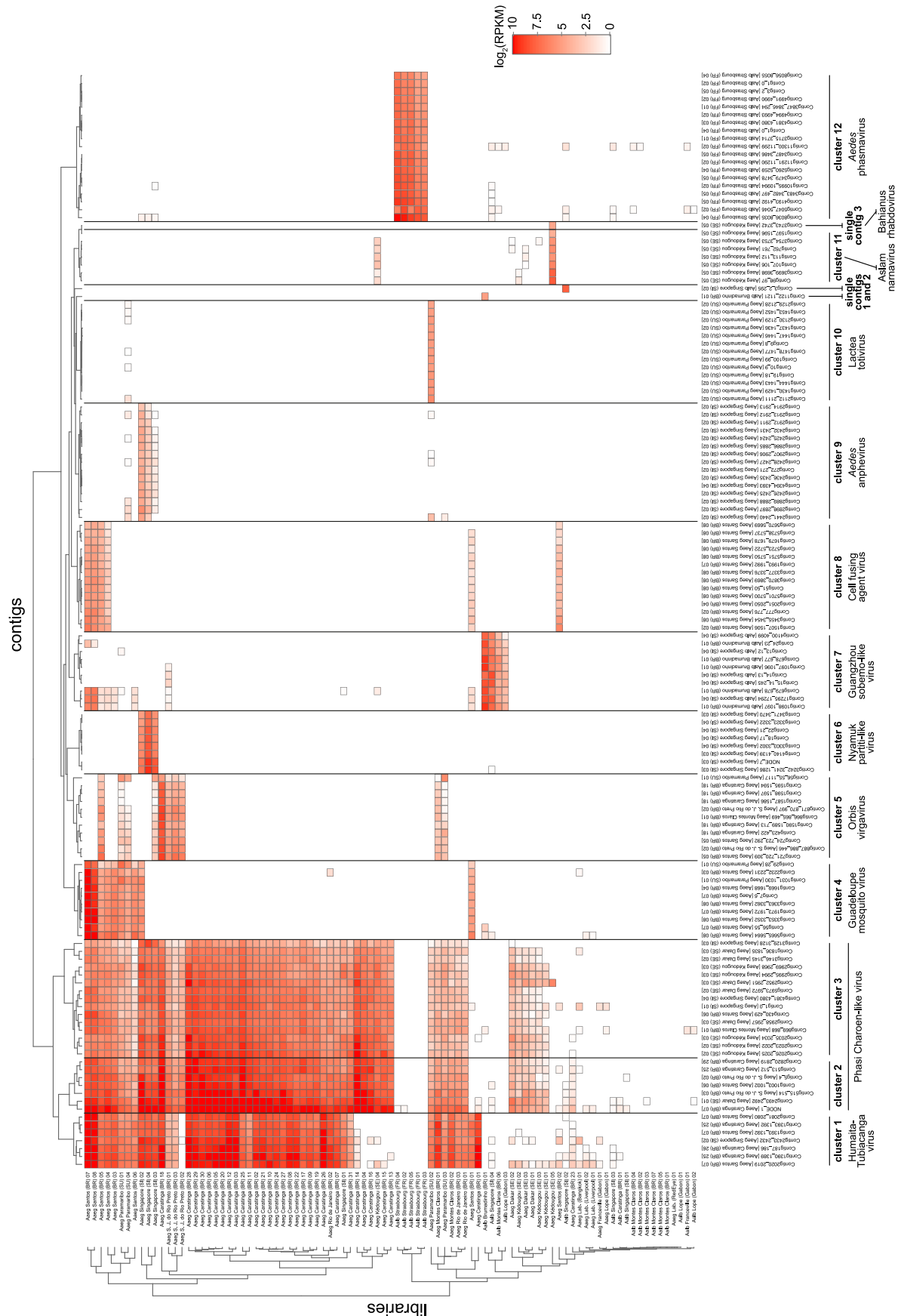
Reprints and permissions information is available at www.nature.com/reprints.

Publisher's note Springer Nature remains neutral with regard to jurisdictional claims in published maps and institutional affiliations.

Springer Nature or its licensor (e.g. a society or other partner) holds exclusive rights to this article under a publishing agreement with the author(s) or other rightsholder(s); author self-archiving of the accepted manuscript version of this article is solely governed by the terms of such publishing agreement and applicable law.

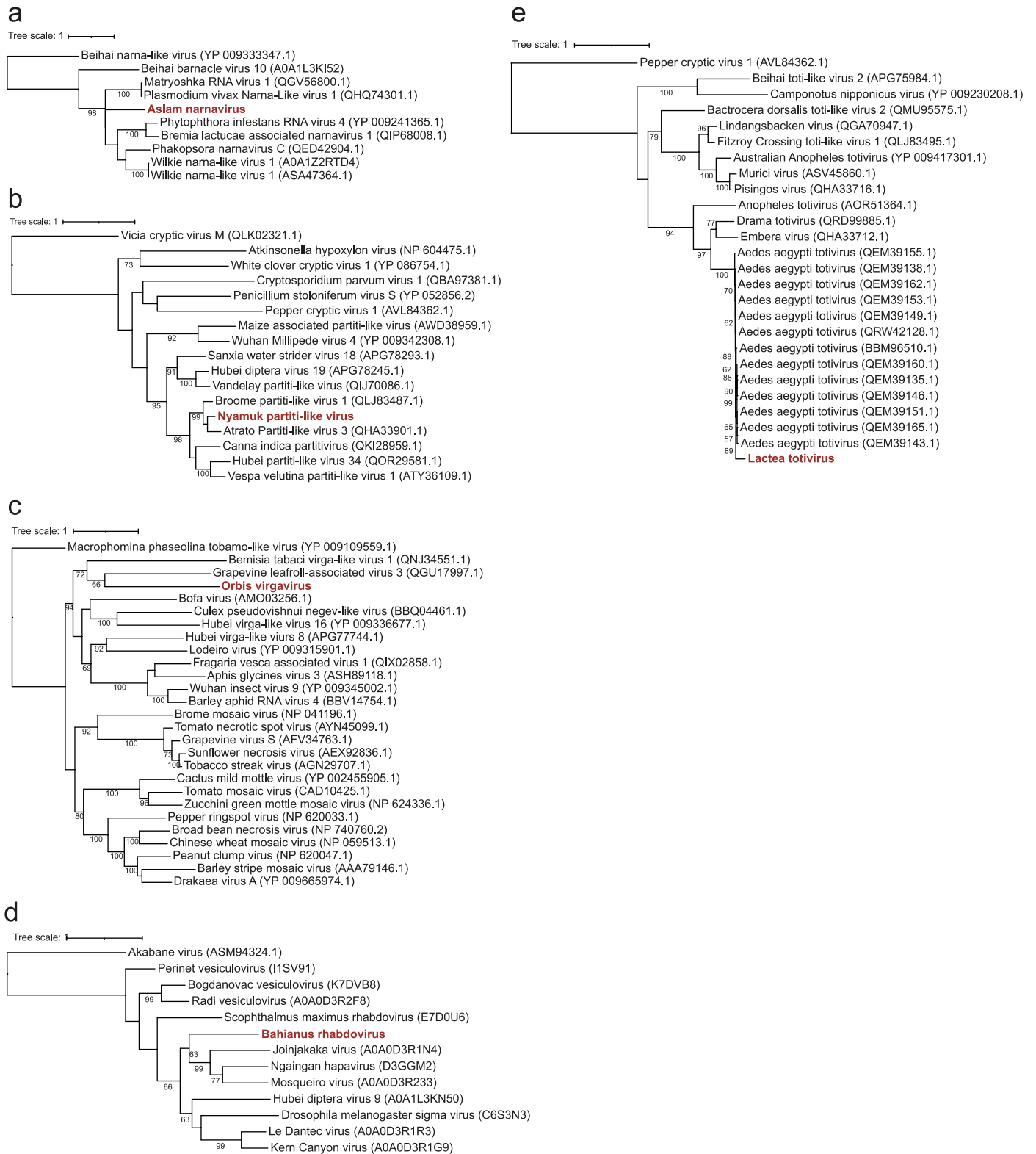
© The Author(s), under exclusive licence to Springer Nature Limited 2023

¹Department of Biochemistry and Immunology, Instituto de Ciências Biológicas, Universidade Federal de Minas Gerais, Belo Horizonte, Brazil. ²Université de Strasbourg, CNRS UPR9022, INSERM U1257, Strasbourg, France. ³Department of Biological Sciences (DCB), Center of Biotechnology and Genetics (CBG), State University of Santa Cruz (UESC), Ilhéus, Brazil. ⁴Mosquitos Vetores: Endossimbiontes e Interação Patógeno-Vetor, Instituto René Rachou-Fiocruz, Belo Horizonte, Minas Gerais, Brazil. ⁵Environmental Health Institute, Vector Biology and Control Division, National Environment Agency, Singapore, Singapore. ⁶Pôle de Zoologie Médicale, Institut Pasteur de Dakar, Dakar, Senegal. ⁷Maladies Infectieuses et Vecteurs: Écologie, Génétique, Évolution et Contrôle (MIVEGEC); Université de Montpellier, Institut de Recherche pour le Développement, CNRS, Montpellier, France. ⁸Laboratoire de Biologie Moléculaire et Cellulaire, Département de Biologie, Université des Sciences et Techniques de Masuku, Franceville, Gabon. ⁹Écologie des Systèmes Vectoriels, Centre Interdisciplinaire de Recherches Médicales de Franceville, Franceville, Gabon. ¹⁰Laboratory of Entomology, Wageningen University and Research, Wageningen, the Netherlands. ¹¹Central Laboratory of the Bureau of Public Health, Paramaribo, Suriname. ¹²Department of Microbiology, Instituto de Ciências Biológicas, Universidade Federal de Minas Gerais (UFMG), Belo Horizonte, Brazil. ¹³Secretaria Municipal de Saúde, Seção de Controle de Vetores, Santos City Hall, Santos, Brazil. ¹⁴Laboratory of Research in Virology, Faculdade de Medicina de São José do Rio Preto (FAMERP), São José do Rio Preto, Brazil. ¹⁵Department of Pathology, University of Texas Medical Branch, Galveston, TX, USA. ¹⁶Department of Infectious and Parasitic Diseases, Faculdade de Medicina da Universidade de São Paulo (FMUSP), Cerqueira Cesar, Brazil. ¹⁷Health Surveillance (Zoonosis Control), Brumadinho City Hall, Brumadinho, Brazil. ¹⁸Center for Biological and Health Sciences, Universidade Estadual de Montes Claros, Montes Claros, Brazil. ¹⁹Centre for Ecology and Conservation, University of Exeter, Penryn Campus, Penryn, UK. ²⁰Institute of Tropical Medicine, Universitätsklinikum Tübingen, Tübingen, Germany. ²¹Lancaster Medical School, Lancaster University, Lancaster, UK. ²²These authors contributed equally: Roenick P. Olmo, Yaovi M. H. Todjro, Eric R. G. R. Aguiar. ✉ e-mail: jtm@ufmg.br



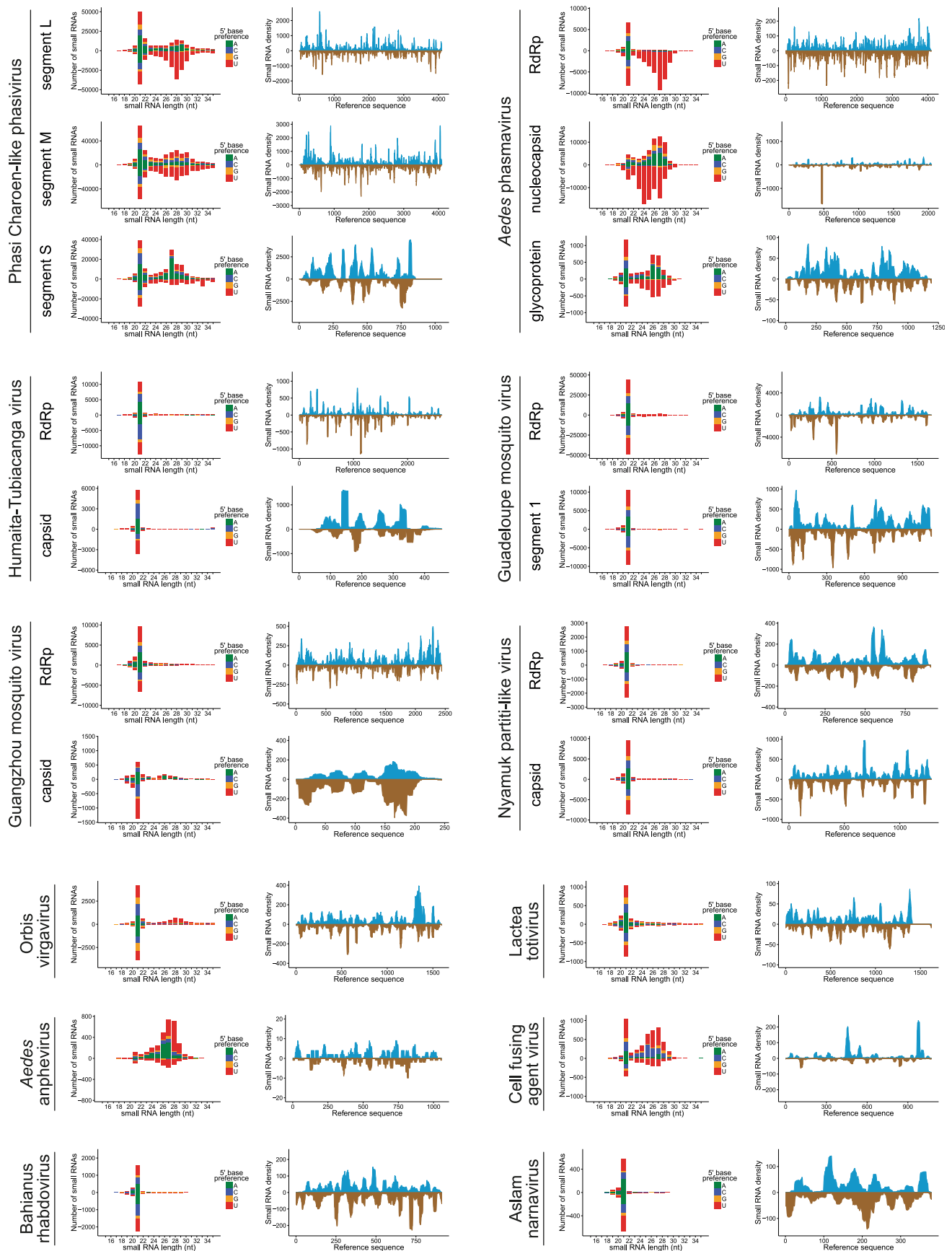
Extended Data Fig. 1 | Co-occurrence of 139 viral contig clusters identified in *A. aegypti* and *A. albopictus* mosquitoes. Heatmap represents the small RNA abundance for each of the 139 viral contigs in our 91 small RNA libraries from *A. aegypti* and *A. albopictus* mosquitoes. White indicates absence of small RNAs

mapping to that contig. Contig clusters were defined using the dendrogram shown on the heatmap. Clusters that had a RdRp sequence were classified as a putative virus. Virus presence was considered if >50% of contigs belonging to a cluster were represented.

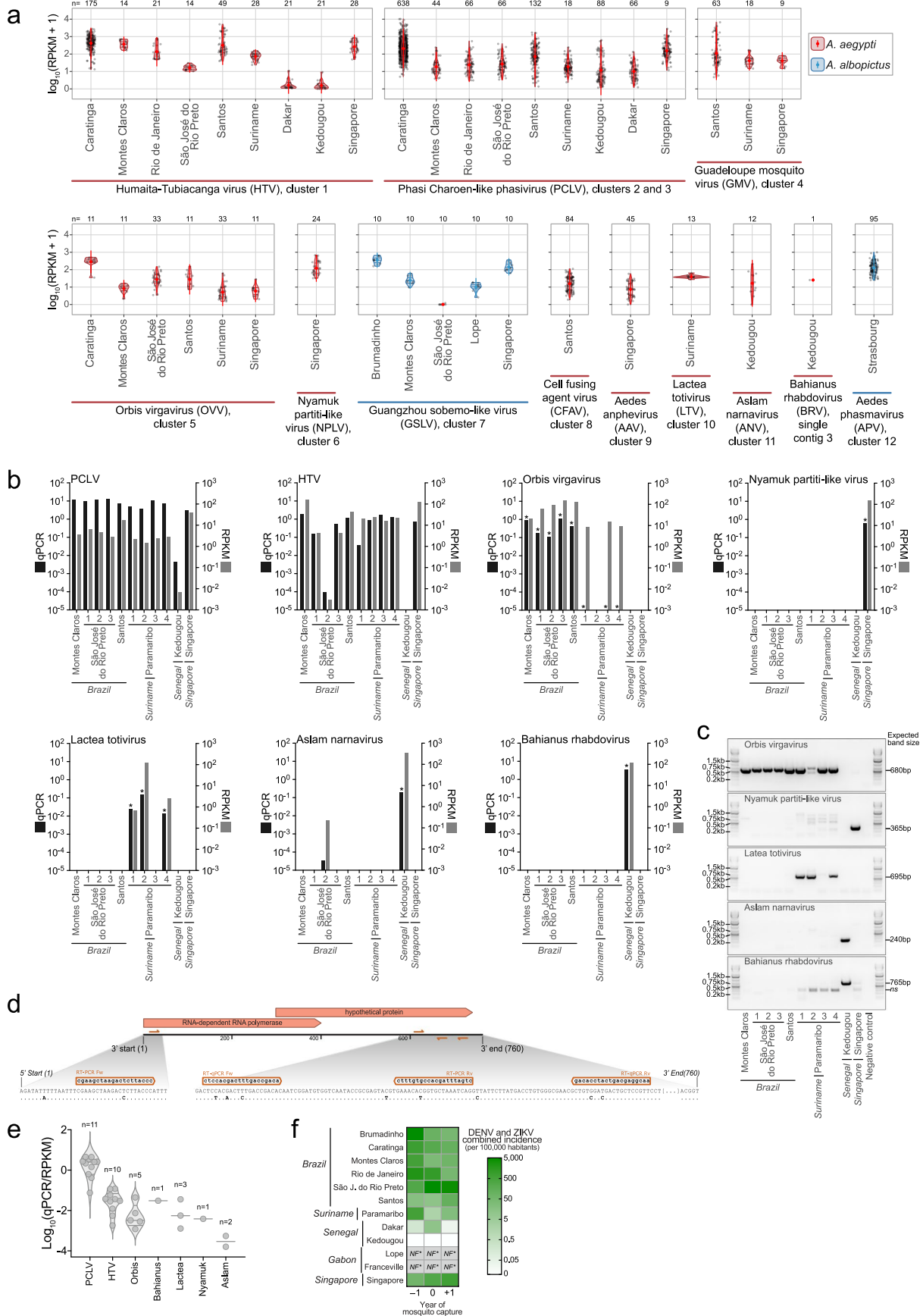


Extended Data Fig. 2 | Phylogeny of viruses identified in *A. aegypti* mosquitoes. Phylogenetic trees were generated using the RdRp amino acid (aa) or nucleotide (nt) sequences and the substitution models as indicated: **a**, Aslam narnavirus (aa - LG + G); **b**, Nyamuk partiti-like virus (aa - BLOSUM 62); **c**, Orbis

virgavirus (aa - BLOSUM62 + F); **d**, Bahianus rhabdovirus (aa - BLOSUM62); **e**, Lactea totivirus (nt - Tamura-Nei 93). Bootstrap confidence is shown close to each clade and values under 60% were omitted.



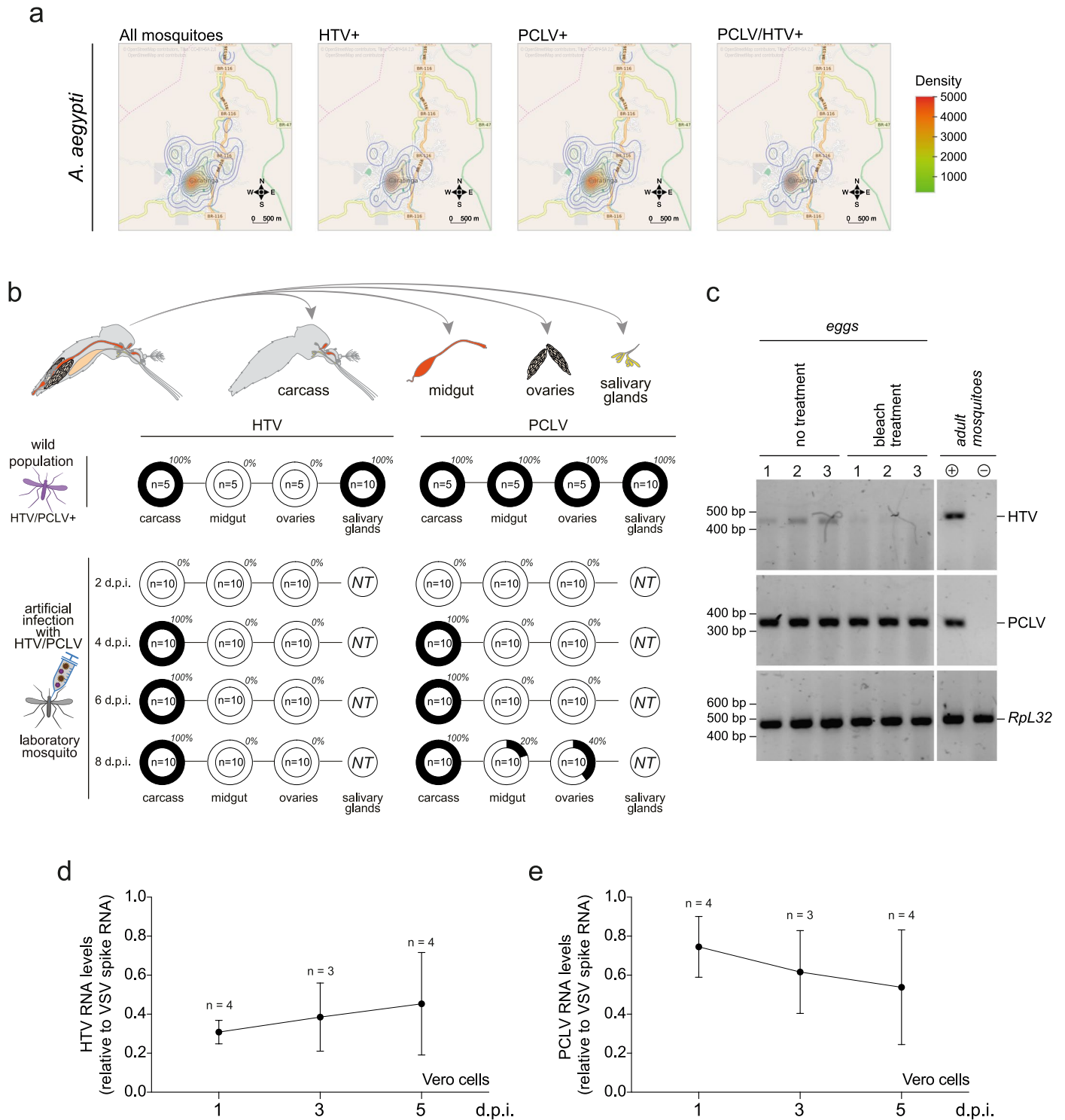
Extended Data Fig. 3 | Virus-derived small RNA profiles in mosquitoes. Small RNA size distribution and 5' base preference is shown on the left while the density of small RNAs (coverage) is shown on the right for representative contig(s) of each of the 12 viruses identified in this study.



Extended Data Fig. 4 | See next page for caption.

Extended Data Fig. 4 | Burden of viruses in mosquitoes from different collection sites. **a**, Abundance of small RNA sequences in pooled libraries from each location. Each dot represents the small RNA abundance in a contig, and violin plots represent contig clusters (see Extended Data Fig. 1) at different locations with colors matching the mosquito species. Error bars represent the standard deviation of the mean for each location. The number of contigs analyzed per location is indicated above each graph. **b**, Detection of representative contigs of newly detected viruses by RT-qPCR (black bars) in comparison to the detection of small RNAs (20-30 nt length) to the same given contig (gray bars). RT-qPCR detection is normalized against the endogenous constitutive gene *RpL32*. *, indicates detection by conventional RT-PCR. **c**, viral

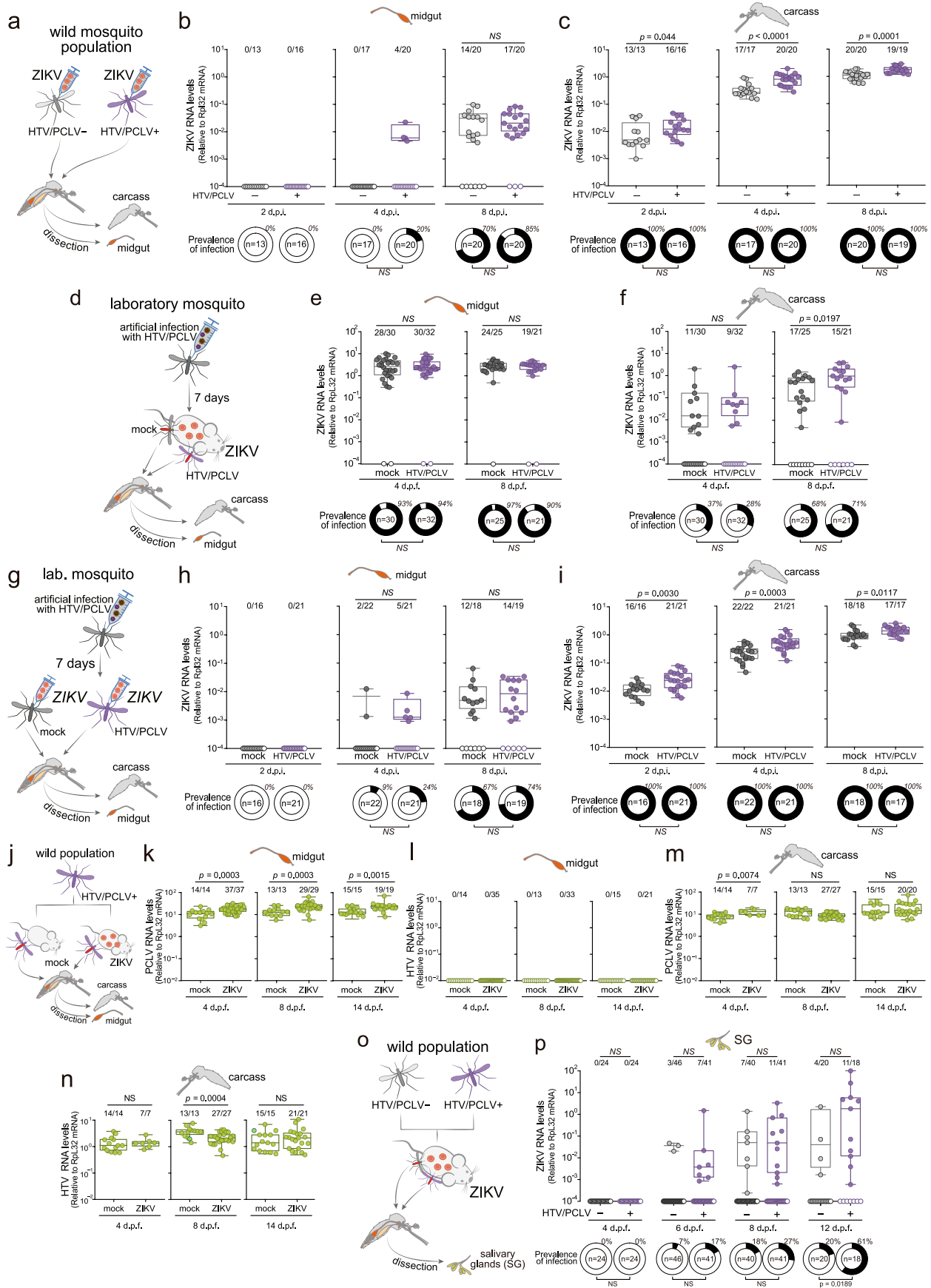
contig detection by conventional RT-PCR using independent sets of primers pairs. Conventional PCR and qPCR were repeated twice on the same samples. The expected size of viral contigs is shown. *ns* indicates a non-specific band. **d**, Sequence variation between viral contigs of Orbis virgavirus in RNA samples originated from Suriname along the region that is complementary to RT-qPCR primers. **e**, Ratio between relative RT-qPCR and small RNA abundance for each virus. The number of independent mosquito samples analyzed per virus is indicated above each graph. **f**, Combined incidence of DENV and ZIKV for each mosquito capture location in the previous, current, and subsequent years of collection (represented by -1, 0, and +1, respectively). Data were obtained from public sources for each location.



Extended Data Fig. 5 | See next page for caption.

Extended Data Fig. 5 | Characterization of HTV and PCLV infection in wild and laboratory mosquitoes. **a**, geographic distribution of mosquitoes carrying HTV and PCLV in the city of Caratinga, Brazil. Maps show the density of adult *A. aegypti* mosquitoes captured from July 2010 until August 2011 estimated from the number of mosquitoes captured in individual traps. All mosquitoes, HTV positive, PCLV-positive and double positive individuals are shown. Virus detection was performed by RT-qPCR. Map source: OpenStreetMap. **b, c** tissue tropism of HTV and PCLV upon natural and artificial infections in *A. aegypti* mosquitoes. **b**, Scheme of mosquito dissection and tissues tested for virus infection by RT-qPCR. Pie charts show the prevalence of HTV and PCLV infection, assessed in tissues of naturally infected wild mosquitoes or laboratory mosquitoes injected with HTV and PCLV. Individual tissues were tested for virus presence upon dissection at 2-, 4-, 6- and 8-days post injection (*d.p.i.*) by RT-qPCR. **c**, Detection of HTV and PCLV in eggs by RT-PCR. Eggs were either rinsed

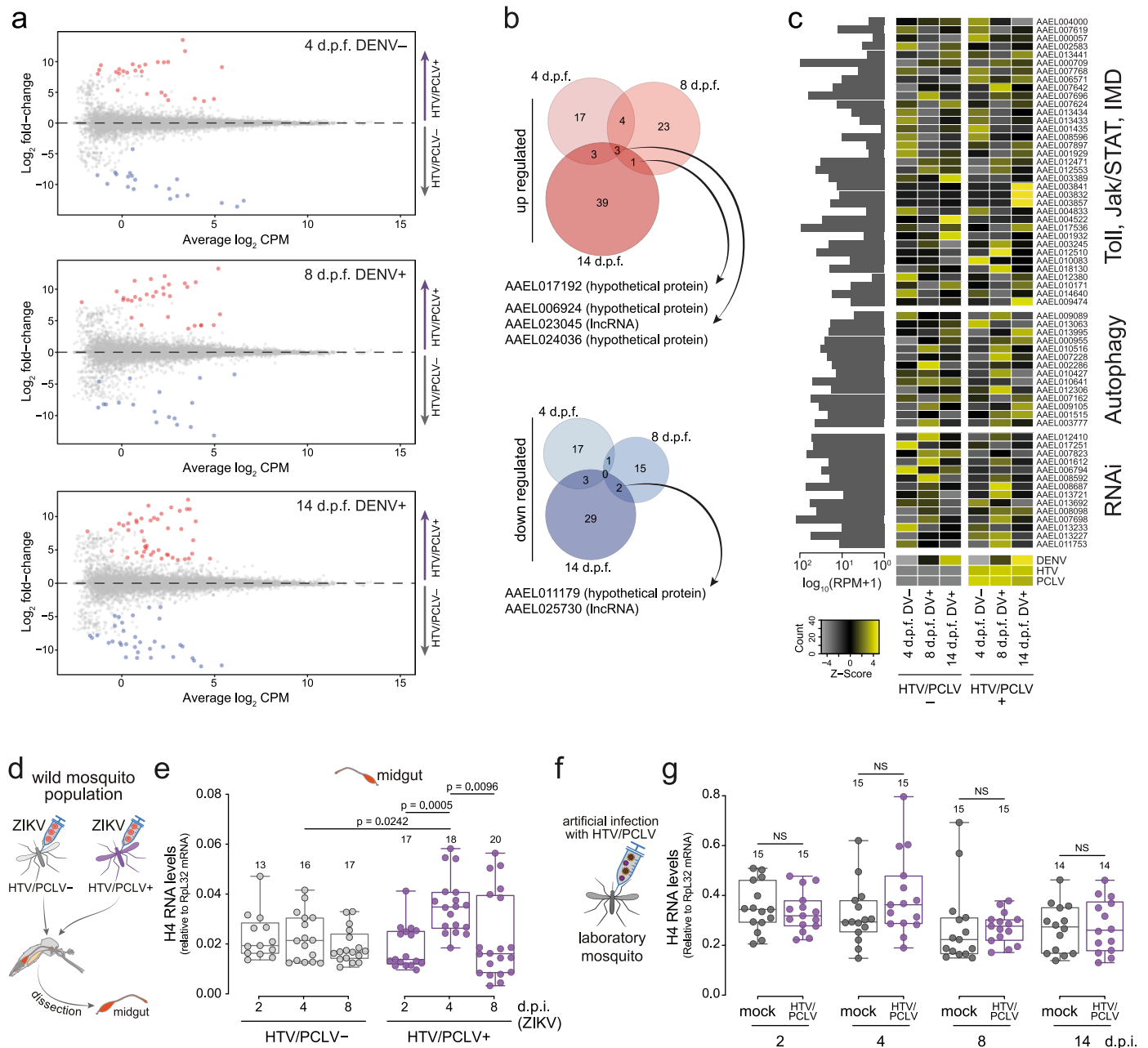
with distilled water (no treatment group) or washed with bleach (2.5% active chlorine) prior to RNA extraction. The endogenous constitutive gene *RpL32* was used as amplification control. Results are representative of two independent experiments. **d-e**, HTV and PCLV do not grow in mammalian cell culture. VERO cells were exposed to mosquito extracts containing HTV (**d**) and PCLV (**e**), and supernatants were collected at 1-, 3- and 5-days post exposure. A spike containing 10^5 pfu of vesicular stomatitis virus (VSV) was added prior RNA extraction and used to normalize the quantification of HTV and PCLV in the supernatant. No statistically significant difference was observed in HTV and PCLV levels at 1-, 3- and 5-days post infection as determined by two-sided one-way ANOVA with Dunns' correction for multiple comparisons. Dots and error bars indicate the mean and the standard error of the mean, respectively. *n* indicates the number of independent tissue culture wells tested for each virus at each time point.



Extended Data Fig. 6 | See next page for caption.

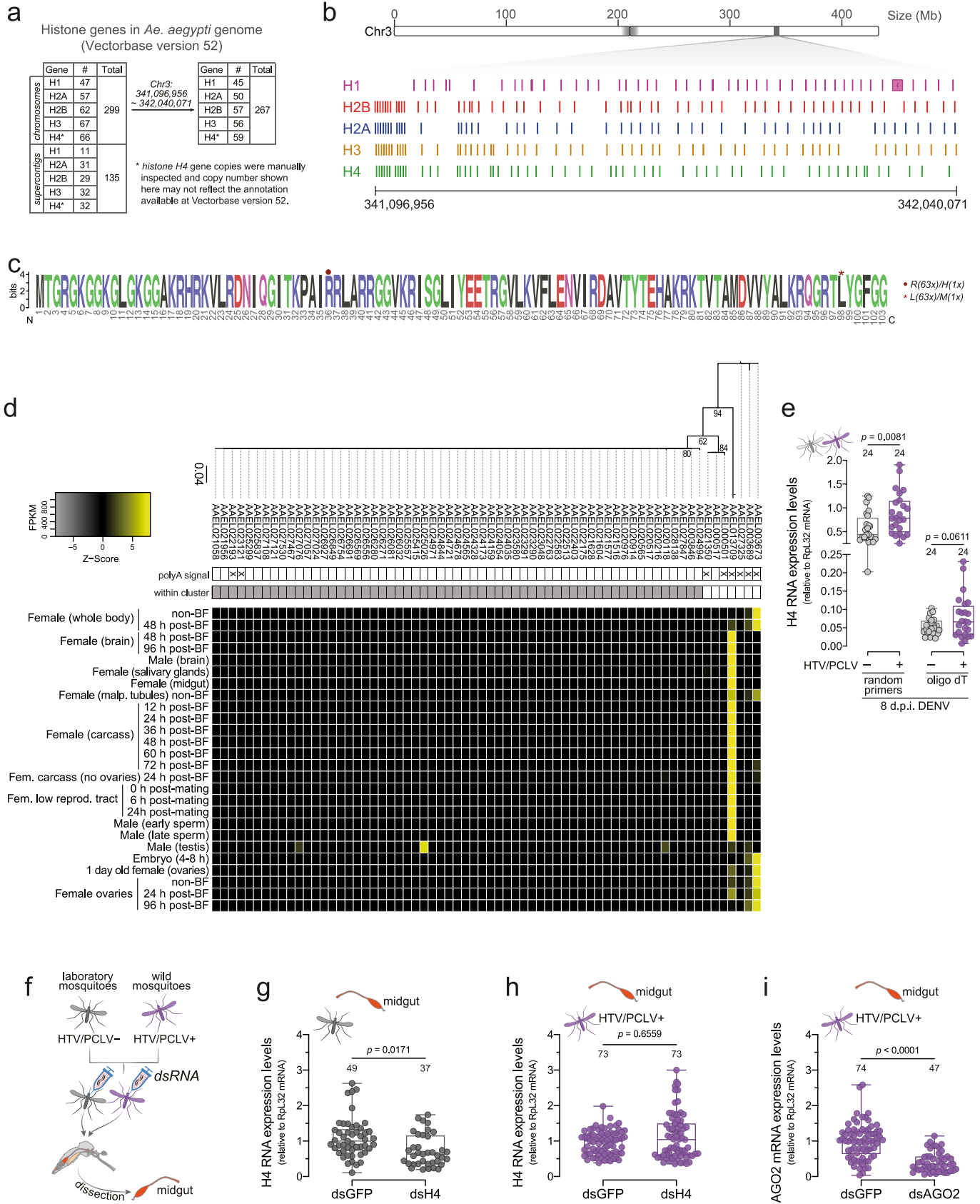
Extended Data Fig. 6 | HTV and PCLV facilitate systemic ZIKV infection in mosquitoes. **a-c**, Strategy to evaluate the interference of HTV and PCLV for ZIKV infection and replication in natural populations of mosquitoes. **(a)** HTV/PCLV-infected and virus-free wild mosquito populations were infected with ZIKV by intrathoracic injection. Viral loads and prevalence of infection were measured in the **(b)** midgut and **(c)** carcass of mosquitoes at 2-, 4- and 8-days post feeding. The prevalence of infection in each group is shown below plots. **d-f**, Laboratory mosquitoes **(d)** were infected artificially with HTV and PCLV and 7 days later were fed on ZIKV-infected mice. Viral loads and prevalence of infection were measured in the **(e)** midgut and **(f)** carcass of mosquitoes at 4- and 8-days post injection. The prevalence of infection in each group is shown below the plots. **g-i**, Laboratory mosquitoes were infected artificially with HTV and PCLV or control (mock) and 7 days later infected with ZIKV by intrathoracic injection. Viral loads and prevalence of infection were measured in the **(h)** midgut and **(i)** carcass of mosquitoes at 2-, 4- and 8-days post injection. The prevalence of

infection in each group is shown below plots. **j-n**, Wild mosquito populations naturally infected with HTV and PCLV were allowed to feed in mice infected with ZIKV or mock-infected controls. Viral loads of HTV and PCLV were measured in the midgut **(k,l)** and in the carcass **(m,n)** of mosquitoes at 4-, 8- and 14-days post feeding. **o-p**, HTV/PCLV-infected or control mosquitoes were exposed to ZIKV-infected mice **(o)**. Viral loads and prevalence of infection were measured in salivary glands **(p)** of mosquitoes at the indicated time points. Pie charts below each group indicate the prevalence of ZIKV infection. *d.p.f.* – days post feeding, *d.p.i.* – days post injection, *NS* – non-significant. In box plots of **b, c, e, f, h, i, k, l, m, n, and p**, boxes show the second and third interquartile ranges divided by the median while whiskers represent maximum and minimum values. Statistical significance was determined by two-tailed Mann–Whitney U-test. Numbers of infected samples over the total number tested are indicated above each column. Each dot represents an individual sample. Statistical significance of prevalence was determined by two-tailed Fisher's exact test.



Extended Data Fig. 7 | Differential gene expression in wild mosquitoes carrying HTV and PCLV. **a**, Differential gene expression in the carcass of wild mosquitoes carrying HTV and PCLV or non-infected siblings during DENV infection at 4, 8 and 14 days post feeding. **b**, number of up or down regulated genes regarding the infection with HTV and PCLV at each time point as shown in **a**. Common genes across time points are shown. **c**, Immune genes regulated during infection with HTV and PCLV in comparison to virus-free siblings at different times after DENV infection. **d-e**, Intrathoracic injection of ZIKV in wild mosquitoes carrying HTV and PCLV or virus free siblings (**d**). Histone H4 levels were quantified in the midgut of mosquitoes at 2, 4, and 8 days post injection with ZIKV (**e**). Error bars represent mean and standard deviations of the mean,

and statistical significance was determined by two-sided one-way ANOVA with Tukey's correction for multiple comparisons. **f-g**, Artificial infection of laboratory mosquitoes with HTV and PCLV does not modulate levels of histone H4. **g**, laboratory mosquitoes were artificially infected with HTV and PCLV and histone H4 levels were analyzed at different time points. In box plots of **e** and **g**, boxes show the second and third interquartile ranges divided by the median while whiskers represent maximum and minimum values. Statistics were performed using two-sided one-way ANOVA with Tukey's correction for multiple comparisons. Each dot represents an individual sample. CPM - counts per million, d.p.i. - days post infection, NS - non-significant.



Extended Data Fig. 8 | See next page for caption.

Extended Data Fig. 8 | Complexity of histone genes in the genome of *A.*

aegypti. **a**, *Histone H4* gene copies in the *A. aegypti* genome (Vectorbase version 52) were reannotated using BLAST similarity search with further confirmation of RNA-seq reads mapping to each gene copy. Along with other *histone* genes currently annotated in Vectorbase, the number of copies in chromosomes or supercontigs are shown and the largest cluster of genes highlighted. **b**, Organization of the largest cluster of histone genes on chromosome 3 as indicated by the gray box. **c**, Weblogo showing the conservation of the amino acid sequence of histone H4 open reading frames, which only varied at the positions 36 and 98, indicated by a circle and an asterisk, respectively. The number of amino acid changes in each position is indicated. **d**, Histone H4 genes organized by nucleotide sequence similarity according to the dendrogram with the expression indicated by the heatmap in different *A. aegypti* tissues. Bootstrap values over 60 are shown. *Histone H4* genes positioned in the cluster at chromosome 3 are indicated by gray boxes and the presence of a polyadenylation signal is indicated. **e**, *Histone H4* gene expression in wild mosquito populations carrying HTV and PCLV or virus free siblings infected with DENV, quantified by RT-qPCR from cDNAs synthesized with random primers (hexamers) or anchored oligo dT₂₂. *d.p.i.*, days post injection. In **d**, SRA accession numbers in same order as shown in the heatmap: Female whole body (non-BF [SRR1585314](#), [SRR1585315](#), [SRR1585316](#); 48 h post-BF [SRR1532683](#), [SRR1532684](#), [SRR1532685](#), [SRR1532693](#), [SRR1532694](#), [SRR1532695](#)); Female brain (48 h post-BF [SRR1166497](#); 96 h post-BF [SRR1167481](#)); Male (brain [SRR1167543](#)); Female salivary glands

([SRR2659965](#), [SRR2659966](#)); Female midgut ([SRR5288077](#), [SRR5288080](#), [SRR5288082](#), [SRR5288087](#), [SRR5288093](#), [SRR5288100](#)); Female malp. Tubules (non-BF [SRR3680433](#), [SRR3680434](#)); Female carcass (12 h post-BF [SRR923823](#); 24 h post-BF [SRR923830](#); 36 h post-BF [SRR923835](#); 48 h post-BF [SRR923841](#); 60 h post-BF [SRR923847](#); 72 h post-BF [SRR923736](#)); Fem. Carcass (no ovaries) 24 h post-BF ([SRR388683](#)); Fem. Low reprod. Tract (0 h post-mating [SRR3213863](#), [SRR3213864](#); 6 h post-mating [SRR3213865](#), [SRR3213866](#); 24 h post-mating [SRR3213867](#), [SRR3213868](#)); Male sperm (early [SRR3554588](#); late [SRR3554589](#)); Male testis ([SRR6311395](#), [SRR6311396](#)); Embryo (4-8 h [SRR1578254](#), [SRR1578255](#), [SRR1578256](#)); 1 day old female ovaries ([SRR388680](#)); Female ovaries (non-BF [SRR1167515](#), [SRR1167516](#), [SRR1167517](#), [SRR1167518](#), [SRR1167519](#), [SRR1167520](#); 24 h post-BF [SRR388682](#); 96 h post-BF [SRR1167538](#), [SRR1167539](#)). **f-h**, silencing of histone H4 by RNA interference in adult mosquitoes. **f**, strategy for dsRNA mediated gene silencing in adult mosquitoes. **g-h**, Histone H4 levels in the midgut of ISV free laboratory mosquitoes (**g**) or wild mosquitoes carrying HTV and PCLV (**h**) injected with dsRNA targeting GFP (dsGFP) as control or histone H4 (dsH4) at 4 days post feeding. **i**, AGO2 levels in the midgut of mosquitoes carrying HTV and PCLV injected with dsRNA targeting GFP (dsGFP) as control or Ago2 (dsAGO2). Each dot represents an individual sample. In box plots of **e**, **g**, **h**, and **i**, boxes show interquartile ranges divided by the median while whiskers represent maximum and minimum values. Statistical significance was determined using two-sided one-way ANOVA with Tukey's correction for multiple comparisons.

Reporting Summary

Nature Portfolio wishes to improve the reproducibility of the work that we publish. This form provides structure for consistency and transparency in reporting. For further information on Nature Portfolio policies, see our [Editorial Policies](#) and the [Editorial Policy Checklist](#).

Statistics

For all statistical analyses, confirm that the following items are present in the figure legend, table legend, main text, or Methods section.

n/a | Confirmed

- The exact sample size (n) for each experimental group/condition, given as a discrete number and unit of measurement
- A statement on whether measurements were taken from distinct samples or whether the same sample was measured repeatedly
- The statistical test(s) used AND whether they are one- or two-sided
Only common tests should be described solely by name; describe more complex techniques in the Methods section.
- A description of all covariates tested
- A description of any assumptions or corrections, such as tests of normality and adjustment for multiple comparisons
- A full description of the statistical parameters including central tendency (e.g. means) or other basic estimates (e.g. regression coefficient) AND variation (e.g. standard deviation) or associated estimates of uncertainty (e.g. confidence intervals)
- For null hypothesis testing, the test statistic (e.g. F , t , r) with confidence intervals, effect sizes, degrees of freedom and P value noted
Give P values as exact values whenever suitable.
- For Bayesian analysis, information on the choice of priors and Markov chain Monte Carlo settings
- For hierarchical and complex designs, identification of the appropriate level for tests and full reporting of outcomes
- Estimates of effect sizes (e.g. Cohen's d , Pearson's r), indicating how they were calculated

Our web collection on [statistics for biologists](#) contains articles on many of the points above.

Software and code

Policy information about [availability of computer code](#)

Data collection	Not applicable.
Data analysis	The following software versions were used in this work: Cutadapt v1.12; Bowtie v1.1.2; Trimmomatic v0.39; Salmon v1.3.0; Perl v5.16.3; BioPerl library v1.6.924; R v3.3.1, v3.6.3 and v4.0.2 (each version is stated in text according to their respective use); R packages EdgeR v3.28.1, ggplot2 v2.2.0 and v3.3.6, venneuler v1.1-3, tidyverse v1.3.1, gplots v3.1.3, fgsea v1.12.0, car v3.1-0, psc1 v1.5.5, SPAdes v3.14.0; CD-HIT v4.8.1; NCBI Conserved Domain Search (CDD v3.18); MAFFT v7 online tool; CIPRES Portal v3.3; MEGA-X tool; iTOL v5.7; T-Coffee v13.45 with the variant M-Coffee; PhyML v3.0 server; GraphPad Prism v9.0.

For manuscripts utilizing custom algorithms or software that are central to the research but not yet described in published literature, software must be made available to editors and reviewers. We strongly encourage code deposition in a community repository (e.g. GitHub). See the Nature Portfolio [guidelines for submitting code & software](#) for further information.

Data

Policy information about [availability of data](#)

All manuscripts must include a [data availability statement](#). This statement should provide the following information, where applicable:

- Accession codes, unique identifiers, or web links for publicly available datasets
- A description of any restrictions on data availability
- For clinical datasets or third party data, please ensure that the statement adheres to our [policy](#)

Small RNA and transcriptome libraries from this study have been deposited on the Sequence Read Archive (SRA) at NCBI under the project accession PRJNA722589. Sequences spanning the RdRP region from newly discovered viruses were deposited on GenBank (accession pending). Other publicly available RNA-seq data sets were obtained from SRA. Accession numbers for small RNA libraries are provided in Extended Data Table 1.

Human research participants

Policy information about [studies involving human research participants and Sex and Gender in Research](#).

Reporting on sex and gender	Unlinked anonymous testing .
Population characteristics	Not applicable.
Recruitment	Unlinked anonymous testing of human blood samples was approved by the ethics committee in research (COEP) of Universidade Federal de Minas Gerais (number 415/04 to EGK). Detailed information about the patients were provided in the original work (Sedda et al, 2018 – ref. 20). No compensation was given to participants.
Ethics oversight	Not applicable.

Note that full information on the approval of the study protocol must also be provided in the manuscript.

Field-specific reporting

Please select the one below that is the best fit for your research. If you are not sure, read the appropriate sections before making your selection.

Life sciences Behavioural & social sciences Ecological, evolutionary & environmental sciences

For a reference copy of the document with all sections, see [nature.com/documents/nr-reporting-summary-flat.pdf](https://www.nature.com/documents/nr-reporting-summary-flat.pdf)

Life sciences study design

All studies must disclose on these points even when the disclosure is negative.

Sample size	No prior sample-size calculation was performed. Considering the non-gaussian distribution of DENV and ZIKV loads in mosquitoes, we opted for larger experiments with usually more than 12 individuals per time-point to increase robustness of the statistical analyses.
Data exclusions	No data points were excluded.
Replication	Experiments were replicated 3 or more times and data points were pooled for presentation and analysis.
Randomization	Mosquitoes were randomly selected from a single cage for each experiment, and were further divided in smaller mosquito groups maintained in separate cages during experiments. All alive mosquitoes available for each time-point were kept for analysis.
Blinding	Researchers were aware of infected and non-infected mice with DENV and ZIKV, or non-infected controls. Mosquitoes containing HTV and PCLV viruses were pooled with virus-free individuals during experiments involving feeding, and identification of mosquitoes from each group occurred after RT-qPCR analysis for each virus. Researchers were aware of mosquito groups containing HTV and PCLV in all other experiments.

Reporting for specific materials, systems and methods

We require information from authors about some types of materials, experimental systems and methods used in many studies. Here, indicate whether each material, system or method listed is relevant to your study. If you are not sure if a list item applies to your research, read the appropriate section before selecting a response.

Materials & experimental systems

n/a	Involvement in the study
<input checked="" type="checkbox"/>	<input type="checkbox"/> Antibodies
<input type="checkbox"/>	<input checked="" type="checkbox"/> Eukaryotic cell lines
<input checked="" type="checkbox"/>	<input type="checkbox"/> Palaeontology and archaeology
<input type="checkbox"/>	<input checked="" type="checkbox"/> Animals and other organisms
<input checked="" type="checkbox"/>	<input type="checkbox"/> Clinical data
<input checked="" type="checkbox"/>	<input type="checkbox"/> Dual use research of concern

Methods

n/a	Involvement in the study
<input checked="" type="checkbox"/>	<input type="checkbox"/> ChIP-seq
<input checked="" type="checkbox"/>	<input type="checkbox"/> Flow cytometry
<input checked="" type="checkbox"/>	<input type="checkbox"/> MRI-based neuroimaging

Eukaryotic cell lines

Policy information about [cell lines and Sex and Gender in Research](#)

Cell line source(s)	Human A549 cells and African green monkey Vero cells were used in this study.
Authentication	None of the cell lines were authenticated.
Mycoplasma contamination	Cells tested negative for mycoplasma.
Commonly misidentified lines (See ICLAC register)	Not applicable.

Animals and other research organisms

Policy information about [studies involving animals; ARRIVE guidelines](#) recommended for reporting animal research, and [Sex and Gender in Research](#)

Laboratory animals	Natural infection with DENV or ZIKV in mosquitoes was performed using AG129 mice deficient for interferon-I and interferon-II receptors (as described by Tan et al, 2010 - doi: 10.1371/journal.pntd.0000672).
Wild animals	Not applicable.
Reporting on sex	All available animals were used regardless of sex.
Field-collected samples	Field traps were used to collect adult mosquitoes that were further identified using morphological characteristics. Locations of mosquito collections are described in the Extended Data Table 1.
Ethics oversight	All procedures involving vertebrate animals were approved by the ethical review committee of the Universidade Federal de Minas Gerais (CEUA 337/2016 and 118/2022). Mosquitoes were collected in Gabon under the research authorization AR0013/17/MESRS/CENAREST/CG/CST/CSAR delivered by CENASREST.

Note that full information on the approval of the study protocol must also be provided in the manuscript.